A module for Rac temporal signal integration revealed with optogenetics

Brian R. Graziano,[1,2] Delquin Gong,[1,2] Karen E. Anderson,[3] Anne Pipathsouk,[1,2] Anna R. Goldberg,[1,2] and Orion D. Weiner[1,2]

[1]Cardiovascular Research Institute and [2]Department of Biochemistry and Biophysics, University of California, San Francisco, San Francisco, CA
[3]The Babraham Institute, Babraham, England, UK

Sensory systems use adaptation to measure changes in signaling inputs rather than absolute levels of signaling inputs. Adaptation enables eukaryotic cells to directionally migrate over a large dynamic range of chemoattractant. Because of complex feedback interactions and redundancy, it has been difficult to define the portion or portions of eukaryotic chemotactic signaling networks that generate adaptation and identify the regulators of this process. In this study, we use a combination of optogenetic intracellular inputs, CRISPR-based knockouts, and pharmacological perturbations to probe the basis of neutrophil adaptation. We find that persistent, optogenetically driven phosphatidylinositol (3,4,5)-trisphosphate (PIP_3) production results in only transient activation of Rac, a hallmark feature of adaptive circuits. We further identify the guanine nucleotide exchange factor P-Rex1 as the primary PIP_3-stimulated Rac activator, whereas actin polymerization and the GTPase-activating protein ArhGAP15 are essential for proper Rac turnoff. This circuit is masked by feedback and redundancy when chemoattractant is used as the input, highlighting the value of probing signaling networks at intermediate nodes to deconvolve complex signaling cascades.

Introduction

Neutrophils are cells of the innate immune system that use chemotaxis to hunt and kill bacteria. To sense small differences in agonist concentration over a wide dynamic range (Zigmond, 1977), components of the neutrophil chemotaxis signaling network adapt to the current level of stimulus (Zigmond and Sullivan, 1979). Adaptation is a general feature of many sensory cascades that reset themselves after responding to a stimulus to measure changes in input rather than absolute levels of input. This behavior dramatically extends the dynamic range of sensory systems. For example, the instantaneous dynamic range of our visual system is five orders of magnitude, but adaptation can adjust this to bracket ambient luminance to enable 14 orders of magnitude in overall brightness detection (Burns and Baylor, 2001).

In the case of chemotaxis, adaptation causes a sustained step input of chemoattractant to generate only transient downstream signaling responses. After this rapid adaptation, cells are sensitive to further changes in agonist concentration (Takeda et al., 2012; Tang et al., 2014). For many sensory cascades, adaptation occurs through stimulus-dependent negative feedback, typically by posttranslational modification of the receptor (Yi et al., 2000; Burns and Baylor, 2001; Porter et al., 2011).

Such mechanisms, however, are dispensable for adaptation and chemotaxis in immune cells (Arai et al., 1997; Hsu et al., 1997) and *Dictyostelium discoideum* (Kim et al., 1997; Xu et al., 2005). Furthermore, the observations that heterotrimeric G protein signaling is neither required for adaptation (Tang et al., 2014) nor exhibits adaptation (Janetopoulos et al., 2001) suggest that adaptation is generated further downstream via mechanisms that remain unknown.

For both neutrophils and *Dictyostelium*, a sustained increase of chemoattractant generates numerous transient downstream signaling responses such as phosphatidylinositol (3,4,5)-trisphosphate (PIP_3) generation (Cadwallader et al., 2002), Rac and Ras activation (Benard et al., 1999; Kae et al., 2004), and actin polymerization (Condeelis et al., 1988), all with half-lives on the order of 30–60 s. Which step or steps of the sensory cascade are responsible for this temporal signal processing? It is tempting to speculate that adaptation originates at the first step exhibiting a transient response and that these temporal dynamics are then passively propagated to downstream nodes. However, the presence of feedback in the signaling cascade complicates this analysis. In neutrophils, for example, PIP_3 and active Rac (Rac-GTP, abbreviated as Rac* in this study) promote actin polymerization, which in turn drives PIP_3 and Rac* activity via mutual positive feedback (Weiner et al., 2002;

Srinivasan et al., 2003; Inoue and Meyer, 2008). Consequently, pinpointing where adaptation is generated in the cascade is not as simple as identifying the most "upstream" signal that adapts after chemoattractant stimulation (Fig. 1 A).

Determining the steps from which adaptation initiates requires more sophisticated tools for bypassing receptor-based signaling to directly control the temporal dynamics of intermediate nodes within this network. Such an approach would enable signaling events transmitted between a given set of nodes to be isolated from parallel pathways and feedback loops that are engaged when cells are stimulated at the level of the receptor. As a result, signal-processing events could be dissected without the confounding effects that normally arise from the simultaneous activation of multiple interacting pathways.

To probe the source or sources of adaptation in neutrophil chemotactic signaling, we used light-responsive phytochrome proteins to modulate the temporal dynamics of signaling intermediates downstream of the receptor (in this study, phosphoinositide 3-kinase [PI3K] activity) in human neutrophil-like HL-60 cells. We demonstrate that local increases in PI3K activity suffice to repolarize cells and guide migration, underscoring the significance of PIP_3-driven signaling events in orienting directed movement. We show that persistent optogenetically driven PIP_3 production results in only transient activation of Rac. Using optogenetic stimulation and CRISPR-based gene knockout, we identified P-Rex1 as the primary stimulator of PIP_3-driven Rac* activation. In addition, we found that ArhGAP15 and actin polymerization both serve as negative regulators of Rac* activity in this circuit. Each of these components plays only a minor role in Rac regulation downstream of chemoattractant; however, all play significant roles in sculpting Rac* activity in response to PIP_3 production. Our findings highlight the value of our optogenetics-based approach in uncovering protein function in pathways with significant feedback and redundancy.

Results

Optogenetics for controlling the timing of PIP_3 production in neutrophils

To simplify the analysis of adaptation in the neutrophil signaling network, we used optogenetic inputs to isolate and interrogate distinct signaling nodes downstream of the receptor. In this study, we focused on the phospholipid PIP_3, which plays a prominent role in the neutrophil signaling network. PIP_3 is sufficient to induce cell polarization in neutrophils (Weiner et al., 2002; Inoue and Meyer, 2008), is necessary for neutrophil polarity in suspension (Ferguson et al., 2007), and is required for neutrophil chemotaxis in vivo (Yoo et al., 2010).

Both PIP_3 and Rac* levels exhibit a transient increase in response to chemoattractant, but because of feedback interactions between PIP_3 and Rac, it is not clear whether transient Rac activity is a cause or consequence of transient PIP_3 generation. This question could be addressed by generating sustained PIP_3 and testing whether Rac* showed sustained or transient dynamics. For this purpose, we modified an optogenetic system we previously used for rapid, reversible control of PIP_3 levels in mouse fibroblasts (Toettcher et al., 2011) for use in human neutrophil-like HL-60 cells. This system relies on a photoswitchable protein, phytochrome B (PhyB), which interconverts between an "open" and "closed" conformation when illuminated with red (~650 nm) or infrared (IR; ~750 nm)
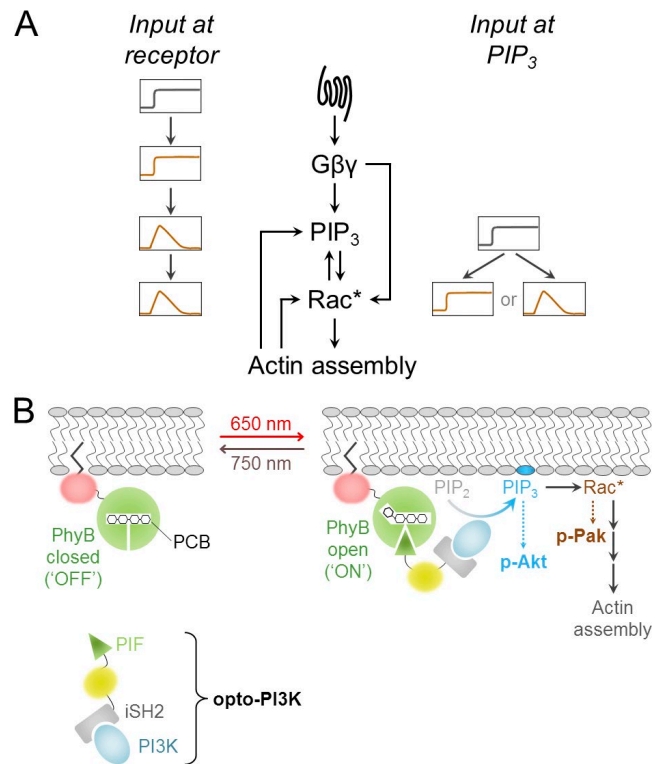
Figure 1. **Probing neutrophil adaptation with optogenetic intracellular inputs.** (A) Schematic of major nodes and interactions within the neutrophil chemotactic signaling cascade. Gray curves indicate sustained inputs at specific points in the cascade, and orange curves indicate time-dependent behavior of downstream nodes. For a delivery of sustained input at the level of PIP_3 production, Rac* could either mimic PIP_3 dynamics or exhibit a transient adaptive response. (B) Optogenetically driven PIP_3 production by phytochrome-based recruitment of endogenous PI3K to the plasma membrane. In immunoblot-based assays, we monitored phospho-Akt and phospho-Pak levels as indirect readouts of PIP_3 generation and Rac activation, respectively. For some assays, we also used MS to directly read out PIP_3 generation as well as PAK-GST pulldown assays to directly assay Rac* activation.

light, respectively (Ni et al., 1999; Levskaya et al., 2009). While in the "open" state, PhyB binds phytochrome-interacting factor (PIF) with high affinity; conversely, switching PhyB into the "closed" state induces dissociation of PIF (Fig. 1 B). PhyB is photoswitchable only when bound to its chromophore, phycocyanobilin (PCB), which we exogenously supply to cells by incubating them in PCB-containing media. In our implementation, HL-60 cells were transduced with (a) membrane-bound PhyB-mCherry-CAAX (hereafter referred to as PhyB) and (b) iSH2-YFP-PIF, which contains the inter-SH2 domain of the p85 regulatory subunit of PI3K. iSH2 constitutively binds the catalytic subunit of PI3K (Dhand et al., 1994). When cells were illuminated with red light, iSH2-YFP-PIF recruited endogenous PI3K to the plasma membrane and catalyzed PIP_3 production (Fig. 1 B). Hereafter, we refer to this complex, which contains the endogenous catalytic subunit of PI3K and exogenous iSH2-YFP-PIF, as "opto-PI3K." Illumination of cells with IR light reversed this process and terminated PIP_3 production.

HL-60 cells are an important model for eukaryotic chemotaxis (Hauert et al., 2002; Artemenko et al., 2014), but only differentiated HL-60s (dHL-60s) can undergo robust polarization and directed migration. Because <20% of dHL-60s retained PhyB expression upon differentiation (Fig. 2 A), we initially

lacked the means to perform optogenetics-based experiments on populations of differentiated cells. However, we recently found that a shorter version PhyB greatly improved its expression in zebrafish (Buckley et al., 2016), and we reasoned that this modification might similarly improve expression in HL-60 cells. To this end, we transduced HL-60s with a truncated PhyB (referred to as "short-PhyB;" Fig. 2 A) that omits the PAS_2 domain present in the PhyB construct used in our earlier mammalian experiments (Levskaya et al., 2009; Toettcher et al., 2011, 2013). Upon differentiation, nearly all dHL-60s retained expression of short-PhyB, a dramatic improvement over our original PhyB construct (Fig. 2 A). We thus used short-PhyB rather than our original PhyB construct to develop our opto-PI3K system for modulating PI3K activity in dHL-60s.

To test the functionality of our optogenetics-based system in neutrophils, we prepared cells in nonadherent squeeze chambers (Malawista and de Boisfleury Chevance, 1997) where the effects of PI3K on cell polarity would be most pronounced (Ferguson et al., 2007). We first verified that opto-PI3K was recruited to the plasma membrane upon red light exposure and dissociated back into the cytosol after illumination with IR light using confocal (Fig. 2, B and C; and Videos 1 and 2) and total internal reflection fluorescence (TIRF) microscopy (Fig. S1 A). These observations demonstrate our ability to control opto-PI3K both rapidly and reversibly.

We next analyzed the behavior of these cells upon repeated turn on and turnoff of opto-PI3K. Cells form pseudopodia (Fig. 2 C, cyan arrowheads, and Videos 1 and 2) when undergoing a turn-on switch from IR to red light (i.e., after recruitment of opto-PI3K to the plasma membrane). These observations are consistent with previous studies showing that uniform increases in PIP_3 are sufficient to induce polarization in quiescent dHL-60s (Weiner et al., 2002; Inoue and Meyer, 2008). Moreover, a turnoff switch from red to IR light frequently coincided with protrusion retraction and depolarization, with cells subsequently forming blebs. These optogenetically induced increases and decreases in cell polarity were rapid and reversible (Fig. 2 D). Opto-PI3K also produced a similar degree of actin polarization as cells stimulated with chemoattractant (Fig. 2, E and F).

Localized PI3K activity spatially directs neutrophil migration

After establishing that global engagement of our opto-PI3K system induces neutrophil polarity (Fig. 2, B–E), we next tested whether this system sufficed to spatially direct neutrophil polarity and movement. Rather than illuminating the entire field of view with either red or IR light, we used a digital micromirror device (DMD) to project a small box of red light onto the trailing edge of a single neutrophil. IR light was simultaneously projected outside this box (Fig. 3 A). This local opto-PI3K engagement sufficed to repolarize neutrophils and trap them in the red box (Fig. 3 B and Videos 3 and 4). Importantly, these effects were dependent on incubating cells with the PhyB cofactor PCB (Fig. S1, B and C). Inverting this light pattern (i.e., projecting IR light into the box) resulted in cells polarizing and migrating away from the box (Fig. 3 B and Video 3). Our spatial experiments demonstrate that localized opto-PI3K activity suffices to control the direction of cell movement and can even overcome existing polarization to activate leading edge formation at the trailing edge. In contrast, previous optogenetic experiments controlling a downstream effector of PIP_3 (Rac*)

for neutrophils in zebrafish found that local stimulation of Rac activity at the rear of polarized cells was insufficient to reorient polarity. However, localized Rac* sufficed to steer/guide a neutrophil by a preexisting front (Yoo et al., 2010). In vitro, PIP_3 activates not only Rac but also other GTPases like Arf to synergistically stimulate actin polymerization (Koronakis et al., 2011). These observations suggest that Rac is sufficient to guide protrusion orientation/growth only where conditions are permissive for leading edge actin polymerization (e.g., within a preexisting protrusion which may contain other active GTPases), whereas PIP_3 suffices to direct the entire polarization program in any location.

Persistently elevated PIP_3 produces only transient Rac activation

After verifying that opto-PI3K produced sufficient PIP_3 to bias neutrophil polarity and motility, we next investigated the temporal dynamics of downstream effectors, particularly activation of Rac GTPase. We first tested whether we could alter the normally transient dynamics of PIP_3 generation that are seen upon chemotactic stimulation. We used mass spectrometry (MS) to directly measure PIP_3 levels in dHL-60s after stimulation with either chemoattractant or sustained red light. Similar to previously reported observations using mouse neutrophils (Deladeriere et al., 2015), cells treated with chemoattractant showed only a transient spike in PIP_3 levels (Fig. 4 A, black curve). In contrast, opto-PI3K cells treated with red light for 10 min showed an increase of PIP_3 at 1 min that remained elevated for the entire time course (Fig. 4 A, red curve). Continuous stimulation of cells using opto-PI3K maintained PIP_3 at a high concentration and overcame the cellular mechanisms that normally lead to PIP_3 adaptation in neutrophils when input is provided at the level of the receptor (Stephens et al., 1993).

Using opto-PI3K to deliver a sustained increase in PIP_3 levels, we next probed the temporal dynamics of Rac activation. We treated quiescent dHL-60s for 5 min with IR light (to ensure that opto-PI3K was in the "OFF" state) followed by 10 min of red light to keep opto-PI3K "ON." Similar experiments were performed in parallel in which dHL-60s were stimulated with chemoattractant rather than opto-PI3K. We measured Rac* levels over this 10-min time course via PAK-GST pulldown assays to enrich for the GTP-bound pool of Rac (Benard et al., 1999), which could then be detected via immunoblotting. If Rac* simply mirrors PIP_3, we would expect sustained PIP_3 to drive sustained Rac activation because, in chemoattractant-treated cells, transient PIP_3 produced transient Rac* (compare black curves in Fig. 4 A to Fig. 4 B). Surprisingly, however, sustained PIP_3 production resulted in only transient activation of Rac* (compare red curves in Fig. 4 A to Fig. 4 B), indicating that the portion of the signaling network lying downstream of PIP_3 is sufficient to produce adaptation in Rac activity.

As an independent means of assessing whether Rac* responds transiently to constant PIP_3 production, we performed additional experiments in dHL-60s with opto-PI3K, and we quantified phosphorylation of Akt at S473 as an indirect readout of PIP_3 (Alessi et al., 1996; Hresko et al., 2003) and phosphorylation of Pak kinase, a Rac effector, as an indirect readout of Rac. In agreement with our direct measurements of Rac* (Fig. 4 B), a step increase of PIP_3 to cells produced only transient phosphorylation of Pak (Fig. 4 C). In contrast, for cells stimulated using chemoattractant, both phospho-Akt and phospho-Pak showed transient responses, as expected (Fig. 4 D). As phospho-Pak
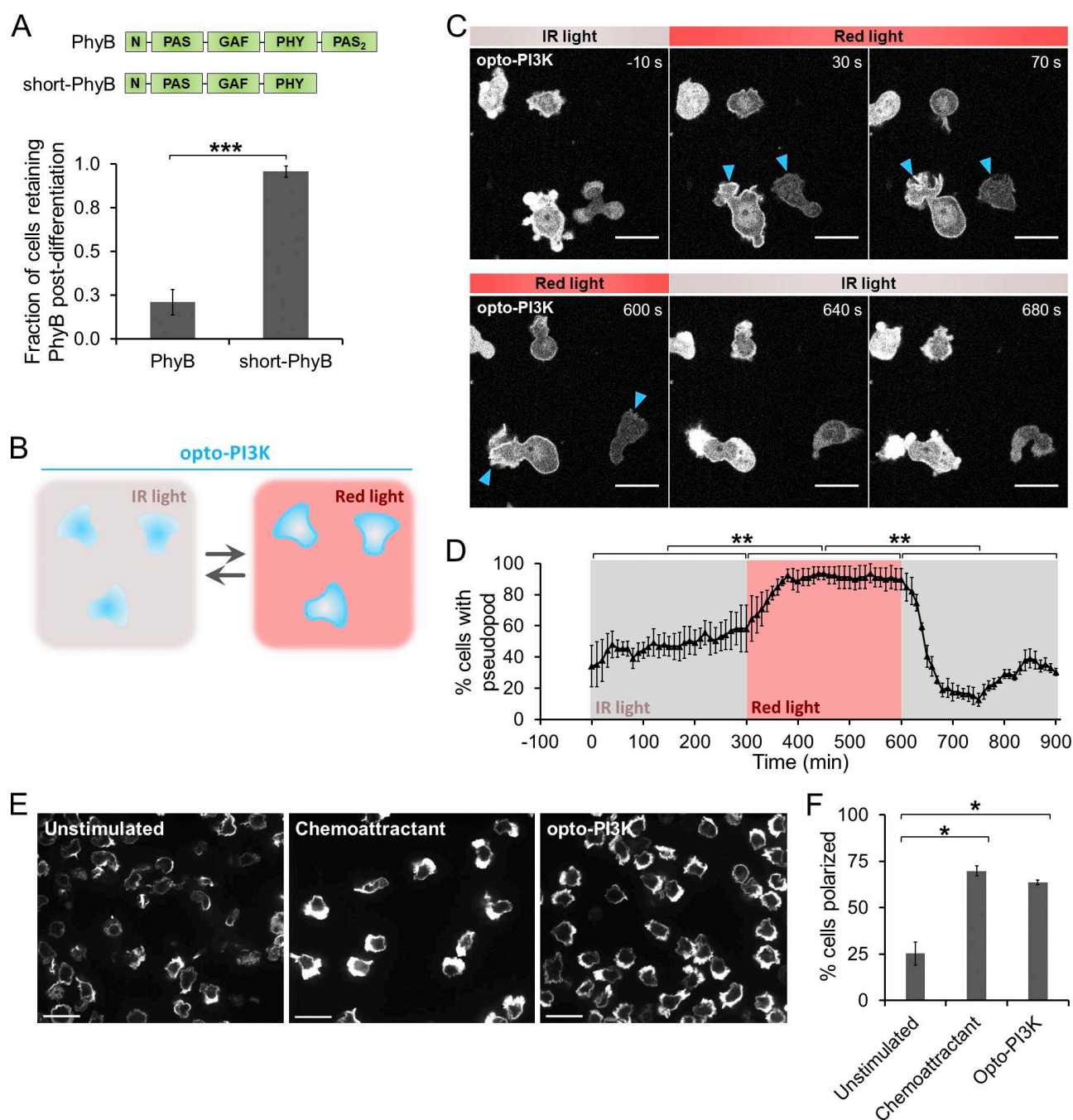
Figure 2. **Development of opto-PI3K for probing neutrophil signaling.** (A, top) Domain layout of PhyB fusion proteins used in this study. "PhyB" is a truncation containing the first 917 residues of PhyB, and "short-PhyB" contains residues 1–621 of PhyB lacking the PAS$_2$ domain. Both PhyB truncations are fused to mCherry-CAAX, as shown in Fig. 1 B. (Bottom) PhyB and short-PhyB expression were determined by measuring mCherry fluorescence via flow cytometry. Each bar represents the mean ratio of PhyB expression in differentiated versus undifferentiated neutrophil-like HL-60 cells. Short-PhyB was much better expressed than PhyB in dHL-60 cells. Data were obtained from at least three independent experiments. Error bars indicate SEM. ***, P < 0.001 by unpaired *t* test. (B) Schematic of experiments shown in C. Whole-field illumination of cells using IR light maintains PhyB in the "OFF" state, causing opto-PI3K (shown in blue) to localize to the cytosol. In contrast, whole-field illumination using red light photoconverts PhyB to the "ON" state, and opto-PI3K translocates to the plasma membrane. This process is reversible (gray arrows). (C) dHL-60s expressing optogenetic components were plated in squeeze chambers. Cells were exposed to alternating rounds of red or IR light as indicated. Images depicting opto-PI3K localization are single focal planes obtained by spinning-disk confocal microscopy. Translocation of opto-PI3K from the cytosol to the plasma membrane was completely reversible, occurred within seconds of exposure to red/IR light, and could be repeated multiple times within the same cell. Cyan arrowheads indicate protrusions formed upon recruitment of opto-PI3K to the plasma membrane. (D) Quantification of percentages of dHL-60s with pseudopods when illuminated with either red or IR light. Cells were prepared as in C. Each point represents the percentage of cells with pseudopods at the indicated time pooled from four independent experiments. Error bars indicate SEM. **, P < 0.01 by paired *t* test. (E) dHL-60s expressing opto-PI3K components were either unstimulated (left), stimulated with 10 nM fMLP for 4 min (center), or treated with red light for 6 min (right) and then fixed and stained for F-actin with phalloidin. Images are single focal planes obtained via spinning-disk confocal microscopy. Bars, 20 µm. (F) Quantification of F-actin polarization phenotypes in dHL-60 cells prepared as described in E. Cells stimulated with opto-PI3K yield a similar degree of polarity as cells stimulated with chemoattractant. Error bars indicate SD. *, P < 0.05 by unpaired *t* test.
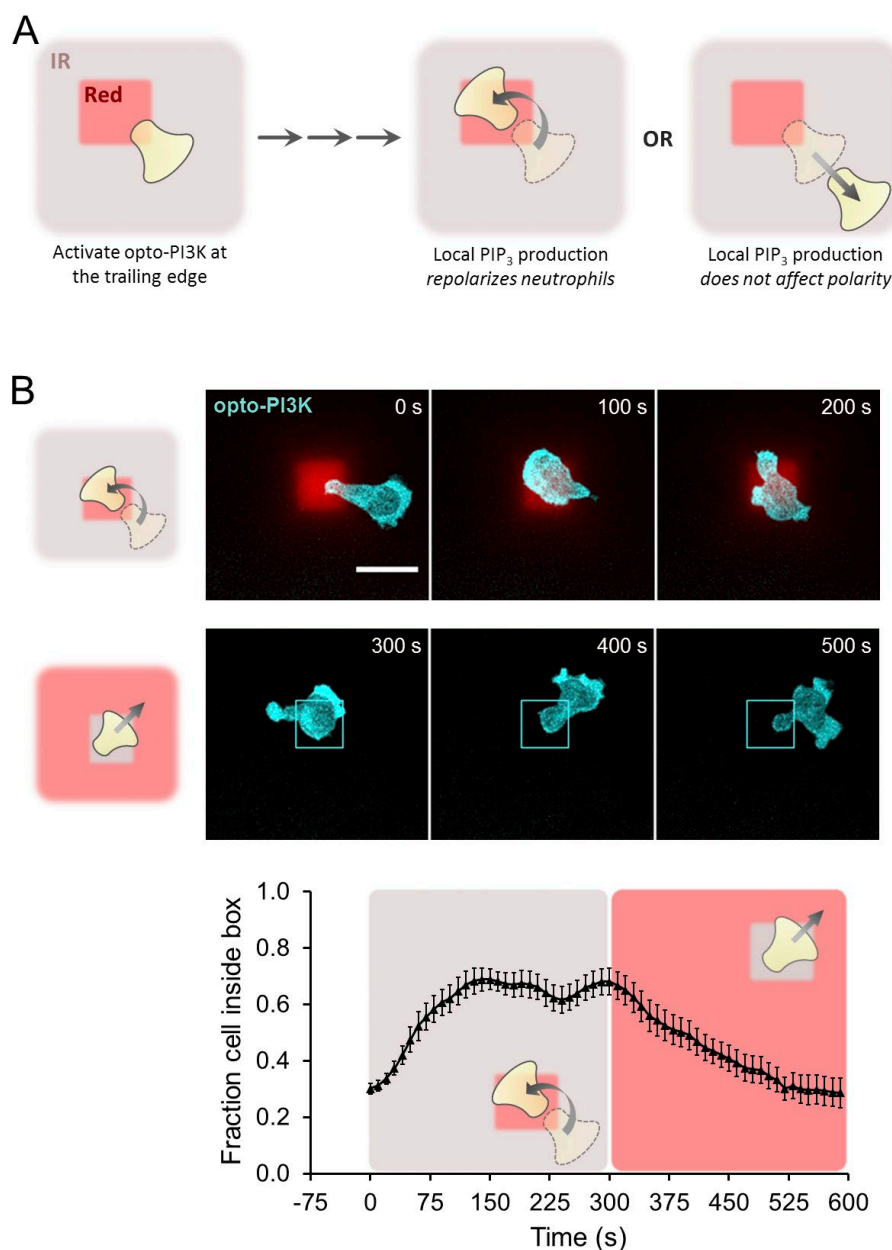
Figure 3. **Localized increases in PI3K activity are sufficient to reorient neutrophil polarity.** (A) Schematic illustrating the experiments shown in B as well as in Fig. S1 (B and C). A square box (~225 µm²) of red light was positioned over approximately the rear third of an actively migrating dHL-60 cell to locally activate PIP$_3$ production while inhibiting it elsewhere with IR light (left). If localized PIP$_3$ production is sufficient to drive neutrophil polarization, the cell should reorient its polarity axis and begin migrating into the box (center). Alternatively, if localized PIP$_3$ production is insufficient, the cell should continue its trajectory away from the box (right). (B) Migrating dHL-60 cells in squeeze chambers were initially exposed to a pattern of red/IR light as depicted in A (top, representative cell). After 5 min, this pattern was "inverted" to suppress opto-PI3K activity in the 225 µm² box but stimulate it everywhere else (middle). The mean cell area lying within the 225-µm² box was plotted over time (bottom). Red/gray shading behind the plot indicates portions of the experiment where opto-PI3K activity was either restricted to or excluded from the 225-µm² box, respectively. Each point represents a mean of 19 different cells measured on three different days. Bar, 20 µm. Error bars indicate SEM.

produced a stronger and more easily quantifiable signal than direct measurements of Rac*, we used this readout as a reporter of Rac* activity in subsequent experiments.

P-Rex1 is required for PIP$_3$-driven Rac activation

We sought to use our optogenetic assay to determine which guanine nucleotide exchange factors (GEFs) function downstream of PIP$_3$ to activate Rac. Because of redundancy, elucidating the suite of Rac GEFs that operate in the full context of chemoattractant stimulation has been difficult. Mouse neutrophils lacking either P-Rex or Vav family GEFs showed only partially impaired Rac stimulation, whereas those lacking both P-Rex1 and Vav1 exhibit compounded defects (Lawson et al., 2011). Similarly, the GEFs Dock2 and Dock5 display partially overlapping roles in promoting Rac activity downstream of chemoattractant (Watanabe et al., 2014). Importantly, chemoattractant receptors use different signaling intermediates to activate these GEFs.

For instance, Gβγ and PIP$_3$ stimulate P-Rex1 (Welch et al., 2002), whereas Src and Syk family kinases stimulate Vav family GEFs (Bustelo, 2014). Prior studies using dHL-60s showed that treatment of cells with PI3K inhibitors only partially impaired chemoattractant-dependent Rac* activity, demonstrating that PIP$_3$-independent pathways act in parallel to regulate Rac (Fuhler et al., 2008; Bréchard et al., 2009). These observations suggest that Rac regulation after optogenetic stimulation of intermediate nodes could operate in a less redundant fashion. Providing an input at the level of PI3K should activate only those Rac GEFs that specifically respond to increases in PIP$_3$. Given that PIP$_3$ serves as one of the primary activators of P-Rex1 (Welch et al., 2002), we hypothesized that P-Rex1 might have a more pronounced role in Rac activation for input delivered at the level of PIP$_3$ production using opto-PI3K rather than input delivered at the level of receptor via chemoattractant (Fig. 5 A).

To test the role of P-Rex in Rac activation, we used CRISPR-mediated genome editing to generate *PREX1-null* dHL-60
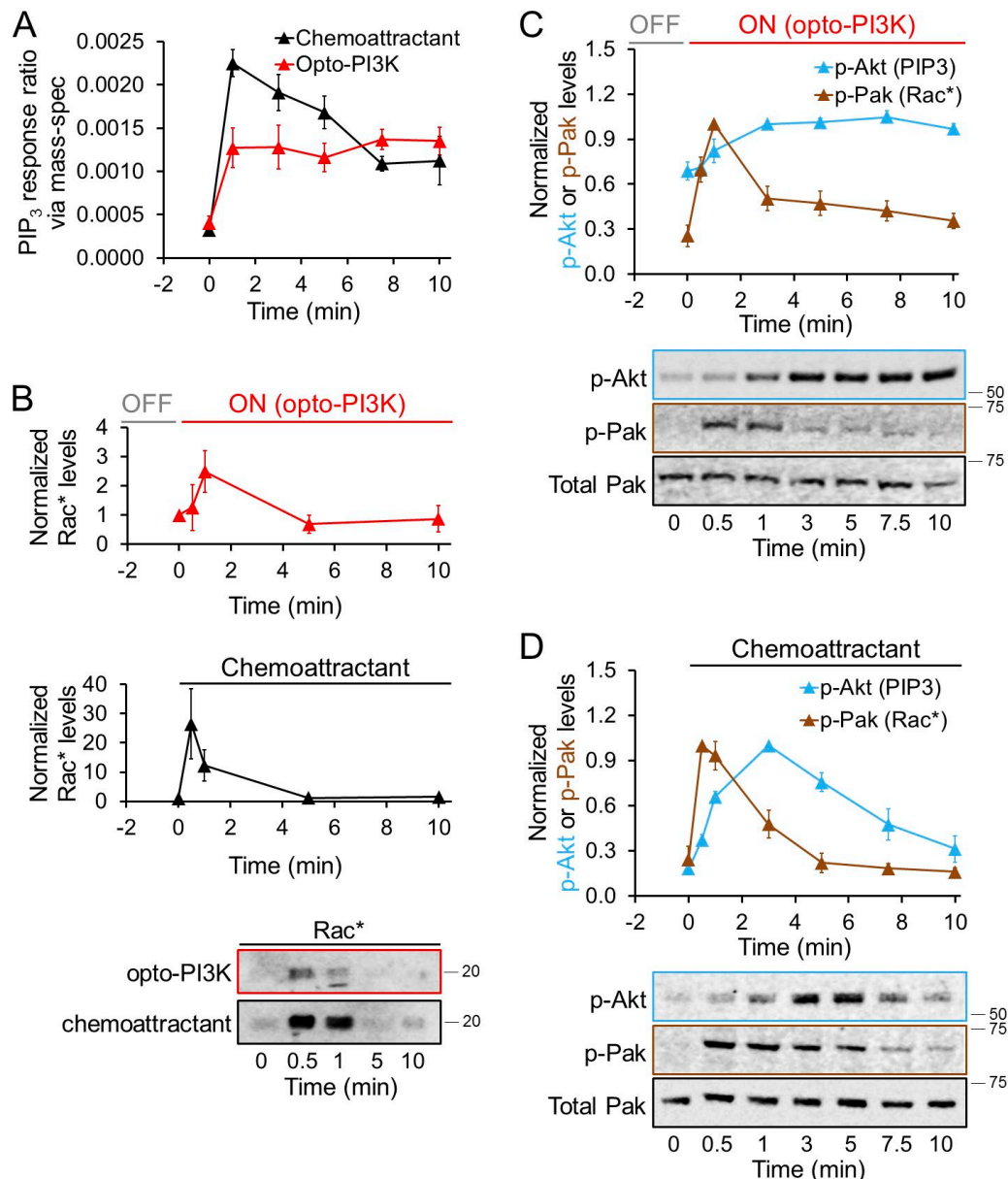
Figure 4. **Sustained PIP$_3$ production generates transient Rac activation.** (A) dHL-60 cells expressing our optogenetic system for controlling PI3K were treated with either 10 nM fMLP (black curve) or red light (red curve) for 10 min. PIP$_3$ levels in each sample were measured using MS. Chemoattractant drove transient increases in PIP$_3$, whereas opto-PI3K drove sustained increases in PIP$_3$. Each point represents a mean of three independent experiments. Error bars indicate SD. (B, top) Cells were placed under inactivating IR light for 5 min followed by exposure to activating red light for 10 min. Rac* was isolated from total cell lysate at indicated time points via Pak pulldown and then quantified via immunoblot using an antibody targeting total Rac. (Middle) Cells were stimulated with 1,000 nM fMLP for 10 min. Samples were collected, processed, and analyzed as in the top panel. Both opto-PI3K and chemoattractant drove transient activation of Rac. (Bottom) Representative immunoblots of total Rac for experiments shown in top and middle panels. For top and middle panels, each point represents a mean of three independent experiments. (C and D, top) Cells were placed under inactivating IR light for 5 min followed by exposure to activating red light for 10 min (C) or treatment with 10 nM fMLP (D). Antibodies targeting phospho-Akt (S473), phospho-Pak, and total Pak were used as PIP$_3$ readouts, Rac* readouts, and loading controls, respectively. The kinetics of these indirect readouts were consistent with the kinetics of our direct readouts of PIP$_3$ and Rac*. Each point represents a mean of three independent experiments. Error bars indicate SEM. (C and D, bottom) Representative immunoblots. Molecular masses are given in kilodaltons.

cells lacking P-Rex1 (Figs. 5 B and S2), the only P-Rex family member expressed in human neutrophils (Donald et al., 2004). *PREX1-null* cells were then transduced with "short-PhyB" and "iSH2-YFP-PIF" for optogenetic control over PI3K. Using MS analysis as in Fig. 4 A, we compared PIP$_3$ levels in unstimulated dHL-60s versus cells stimulated with either chemoattractant or opto-PI3K. Both types of input resulted in a three- to fourfold increase in PIP$_3$ levels, indicating that loss of P-Rex1 did not affect PIP$_3$ production (Fig. 5 C).

We next measured Rac* in *PREX1-null* cells and observed only a weak Rac* response to our opto-PI3K input (Fig. 5 D), indicating that P-Rex1 plays a dominant role in PIP$_3$-stimulated Rac activation. In contrast with our observations in opto-PI3K-stimulated cells, both WT and *PREX1-null* cells treated with *N*-formylmethionine-leucyl-phenylalanine (fMLP) showed nearly identical timing and magnitude of phospho-Pak activity over the 10-min time course (Fig. 5 E). We also observed similar results in a *PREX1-null–2* line generated with a different guide RNA (gRNA;
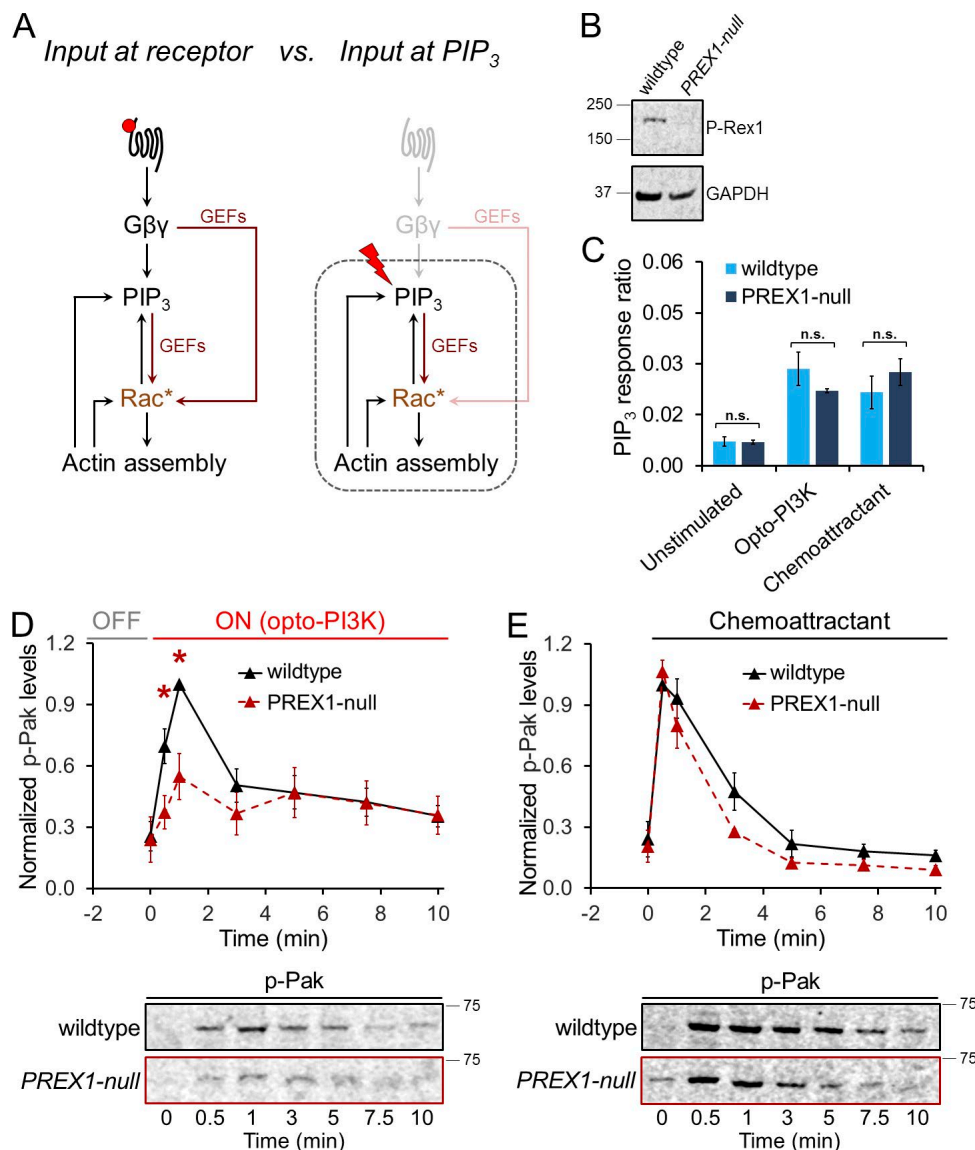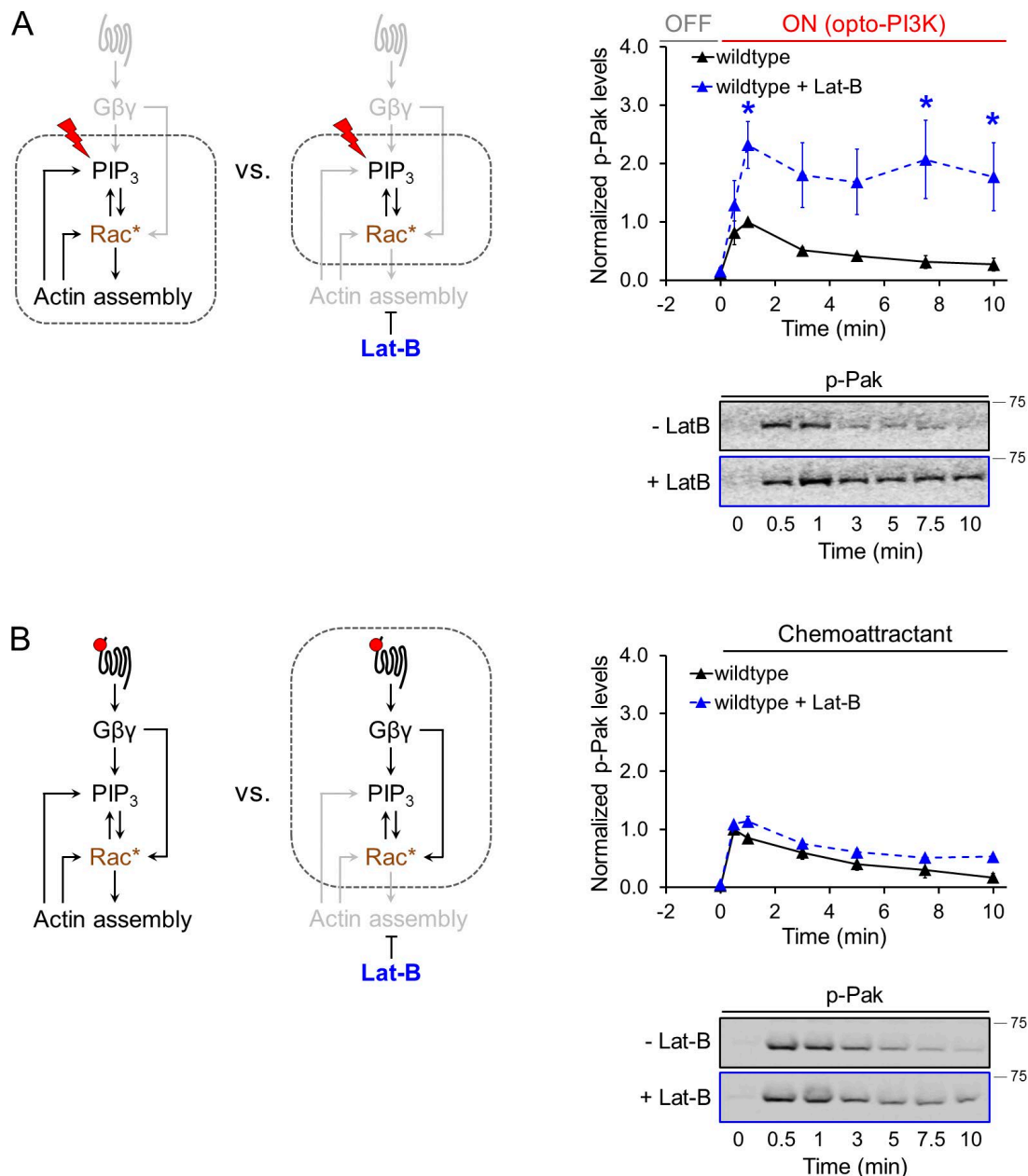
Figure 5. **P-Rex1 is a dominant GEF for PIP$_3$-driven Rac activation.** (A) Schematics for experiments described in C–E. Stimulation using chemoattractant and opto-PI3K is represented by a red circle and red lightning bolt, respectively. Red lines indicate links in the cascade where Rac GEFs participate in signal transduction. By delivering an input specifically at the level of PIP$_3$ (right), only PIP$_3$-stimulated Rac GEFs (dark red line) should participate in Rac activation. (B) P-Rex1 antibody immunoblots of WT and *PREX1-null* cells. GAPDH was used as a loading control. (C) MS analysis of PIP$_3$ in WT or *PREX1-null* cells. Cells were collected before treatment ("Unstimulated") after exposure to red light for 2 min ("opto-PI3K") or incubation with 10 nM fMLP for 1 min ("Chemoattractant") and were processed as described in Fig. 4 A. Each bar represents a mean of three independent trials. Loss of P-Rex1 did not significantly affect PIP$_3$ production. Error bars indicate SD. n.s., $P > 0.05$ by unpaired t test. For both WT and *PREX1-null* cells, the difference in PIP$_3$ levels between unstimulated cells and cells stimulated with either fMLP or opto-PI3K is significant ($P < 0.05$ by unpaired t test). (D and E) WT (black curves) or *PREX1-null* (red dashed curves) cells were treated with either red light (D) or 10 nM fMLP (E) for 10 min. Rac* was measured as in Fig. 4 C. Each point represents a mean of three independent experiments. Rac activation was significantly decreased in *PREX1-null* cells. Error bars indicate SEM. *, $P < 0.05$ by unpaired t test. Immunoblots depict one representative experiment. Molecular masses are given in kilodaltons.

Fig. S3), indicating that the Rac* activation defects we observed upon loss of P-Rex1 do not arise from off-target CRISPR editing or bottlenecks created during single-cell cloning. Collectively, our observations indicate that P-Rex1 is required for full activation of Rac* downstream of PIP$_3$, whereas other GEFs acting in PIP$_3$-independent pathways can compensate for the loss of P-Rex1 when input is provided at the level of the receptor.

Actin assembly is required for proper turnoff of PIP$_3$-driven Rac* activity

After identifying P-Rex1 as a major regulator of PIP$_3$-driven Rac activation, we next focused on identifying factors that are

required for the termination of Rac activation after sustained production of PIP$_3$. F-actin is generally thought of as being one of the most "downstream" nodes of the chemotaxis signaling network. However, F-actin provides feedback to multiple nodes lying within "upstream" portions of the cascade (Fig. 6 A, left; Weiner et al., 2007; Inoue and Meyer, 2008; Huang et al., 2013). To determine whether F-actin–dependent processes play a role in Rac turnoff, we first treated cells with latrunculin B to inhibit actin assembly (thus preventing actin-dependent feedback; Coué et al., 1987) and then subjected these cells to a step increase of PIP$_3$. In this context, optogenetics enabled us to bypass upstream receptor-based signaling, and pharmacology
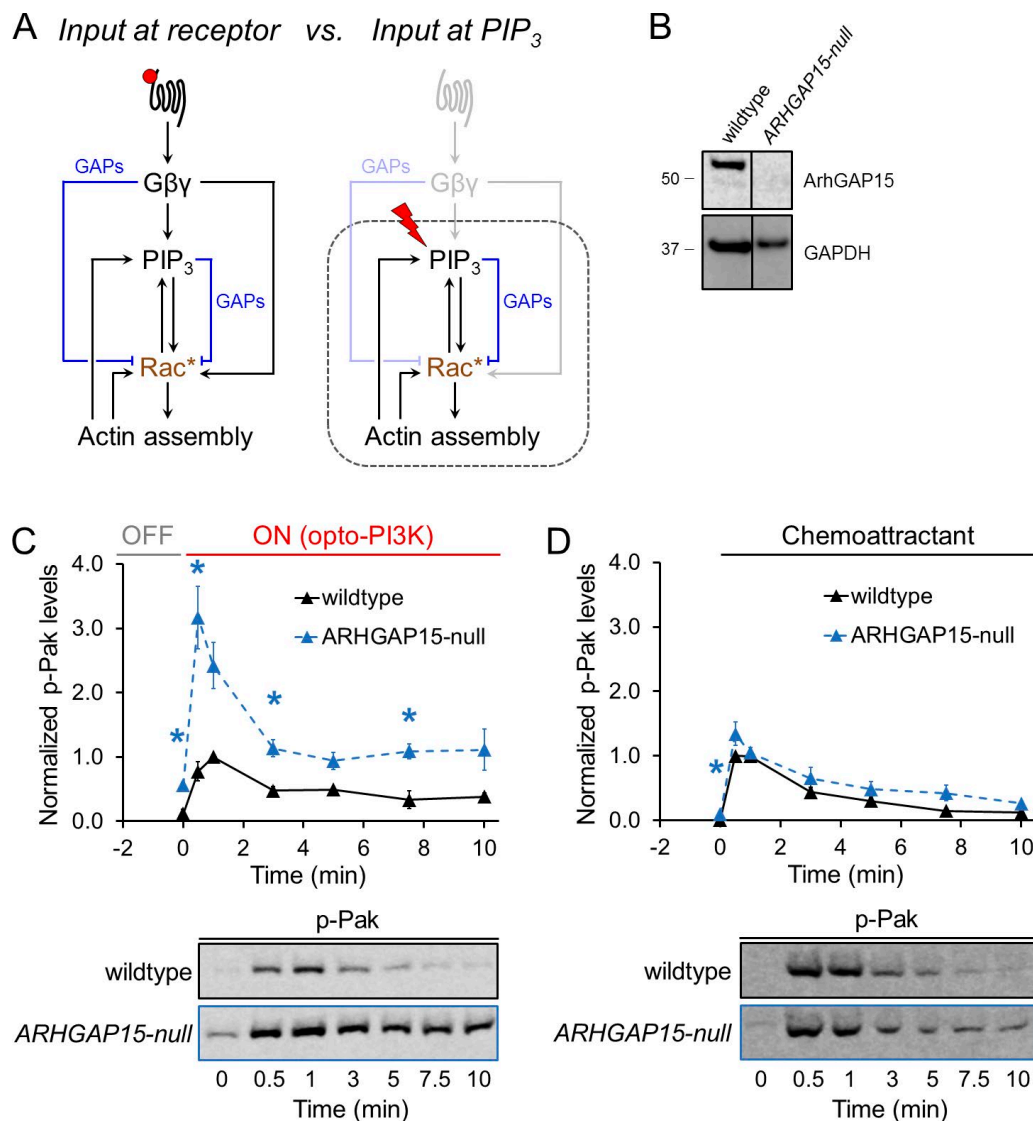
Figure 6. **Actin polymerization is essential for Rac turnoff downstream of opto-PI3K.** (A and B, left) Schematics for experiments described in right panels. Stimulation using chemoattractant and opto-PI3K is represented by red circles and red lightning bolts, respectively. (A and B, right) WT cells in the absence (black curves) or presence of an actin polymerization inhibitor (10 µM latrunculin B [Lat-B], blue dashed curves) were treated with red light (A) or 10 nM fMLP (B) for 10 min. Rac* was measured as in Fig. 4 C. Each point represents a mean of four independent experiments. A loss of actin polymer significantly inhibited Rac turnoff downstream of opto-PI3K but had no significant effect on Rac activity for chemoattractant-stimulated cells. Error bars indicate SEM. *, P < 0.05 by unpaired *t* test. Immunoblots depict one representative experiment. Molecular masses are given in kilodaltons.

enabled us to bypass downstream feedback interactions from the actin cytoskeleton. Strikingly, with actin polymerization blocked, sustained increases in PIP$_3$ produced sustained, rather than transient, increases in Pak phosphorylation, with a significantly higher amplitude of phospho-Pak levels (Fig. 6 A, right). However, when we stimulated latrunculin-treated cells with chemoattractant, we observed only a mild defect in Rac* amplitude and turnoff, as assessed by phospho-Pak levels (Fig. 6 B). These results demonstrate that actin polymer plays a key role in terminating Rac* after a persistent PIP$_3$ input and that F-actin–dependent processes set both the amplitude and duration of PIP$_3$-driven Rac* activity.

During our analysis of the role of P-Rex1 in Rac activation, we noted that stimulation of *PREX1-null* cells with opto-PI3K still produced a small amount of Rac* activity (Fig. 5 D). This observation suggests that other GEFs may function alongside P-Rex1 and play a secondary role in linking PIP$_3$ production to Rac activation. To sensitize our ability to detect these GEFs, we used latrunculin to impair Rac turnoff. Under these conditions, *PREX1-null* cells, which had been defective in Rac* activation in the presence of F-actin (Fig. S4; compare red and gray curves), now showed potent PIP$_3$-driven phospho-Pak production in the absence of F-actin (Fig. S4, blue curve). Although multiple GEFs appear to function in parallel to activate Rac in

Figure 7. **ArhGAP15 is essential for Rac turnoff downstream of opto-PI3K.** (A) Schematics for experiments described in C and D. Stimulation using chemoattractant and opto-PI3K is represented by a red circle and red lightning bolt, respectively. Blue lines indicate links in the cascade where Rac GAPs participate in signal transduction. By delivering an input specifically at PIP_3 (right schematic), only Rac GAPs that respond to PIP_3 generation (dark blue lines) should participate in Rac* deactivation. (B) Immunoblots of WT and *ARHGAP15-null* cells using an antibody targeting ArhGAP15. GAPDH was used as a loading control. Black lines indicate that intervening lanes have been spliced out. (C and D) WT (black curves) or *ARHGAP15-null* (blue dashed curves) cells were treated with either red light (C) or 10 nM fMLP (D) for 10 min. Rac* was measured as in Fig. 4 C. Each point represents a mean of three independent experiments. A loss of ArhGAP15 inhibited Rac turnoff downstream of opto-PI3K but not for chemoattractant-stimulated cells. Error bars indicate SEM. *, P < 0.05 by unpaired *t* test. Immunoblots depict one representative experiment. Molecular masses are given in kilodaltons.

response to PIP_3 increases, P-Rex1 plays a dominant role when the normal Rac turnoff mechanisms are intact.

ArhGAP15 functions independently of actin assembly to turn off PIP₃-driven Rac* activity

After identifying the GEF P-Rex1 as a dominant regulator of PIP_3-driven Rac activation, we next sought to determine the GTPase-activating proteins (GAPs) required for Rac* turnoff. Similar to our rationale for focusing on P-Rex1, we reasoned that only a subset of Rac GAPs activated in response to chemoattractant would be engaged downstream of PIP_3 production (Fig. 7 A). We focused on GAPs known to be active against purified Rac* and whose recruitment to the plasma membrane depends on PI3K activity. The GAPs ArhGAP15 and SH3BP1

both satisfy these conditions (Cicchetti et al., 1995; Seoh et al., 2003; Costa et al., 2007; Schlam et al., 2015).

To assess the roles of each of these GAPs in modulating PIP_3-driven Rac* activity, we used CRISPR-mediated gene editing to generate *ARHGAP15-null* (Fig. 7 B) and *SH3BP1-null* (Fig. S6 A) lines in HL-60s expressing our opto-PI3K components. When treated with opto-PI3K, *ARHGAP15-null* cells displayed significantly higher levels of Rac* activity, which remained elevated throughout the 10-min time course (Fig. 7 C). In contrast, Rac* activity in chemoattractant-treated cells was indistinguishable from WT cells (Fig. 7 D). To verify that loss of ArhGAP15 does not increase Rac* through potentiation of PIP_3 production, we quantified phospho-Akt levels by immunoblot to indirectly read out PIP_3 levels in our samples and found that opto-PI3K activity was not significantly changed in
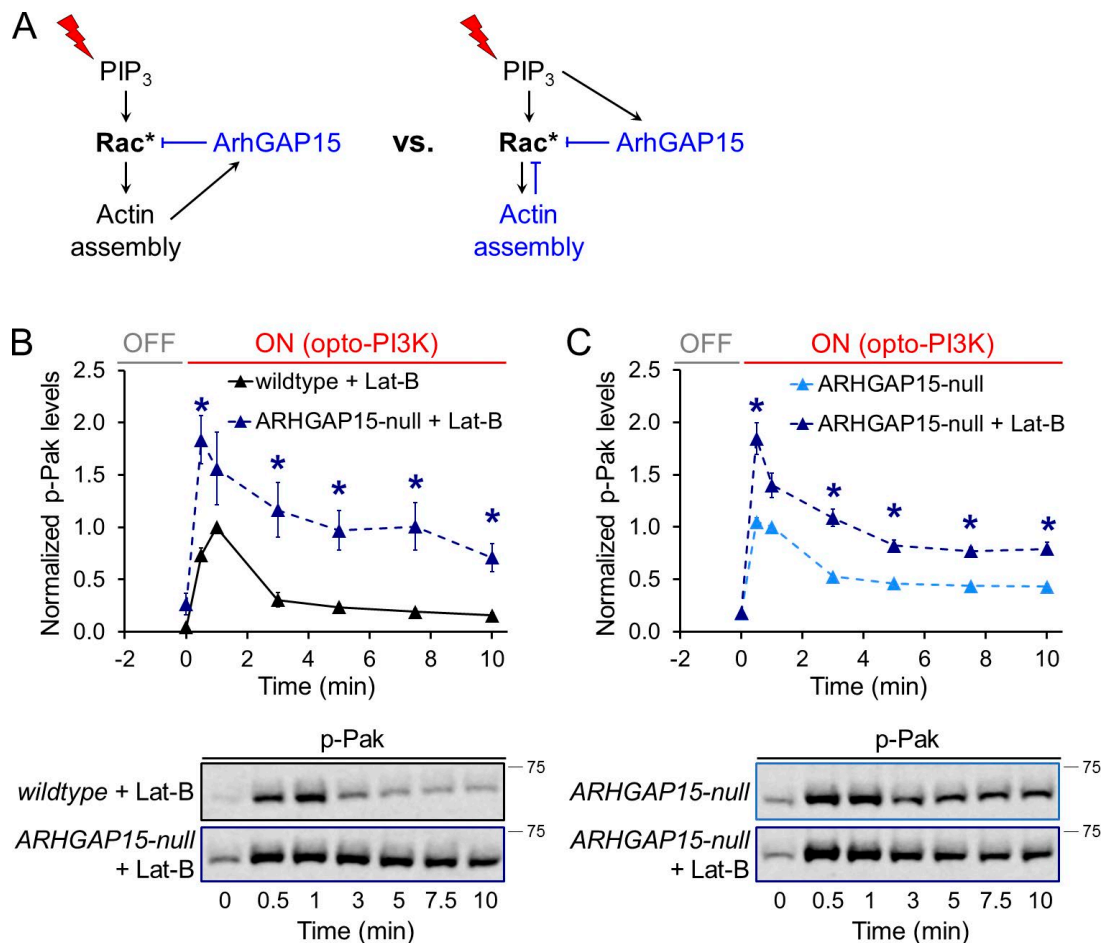
Figure 8. **ArhGAP15 and actin polymerization are parallel routes for Rac turnoff downstream of opto-PI3K.** (A) ArhGAP15 could act downstream of actin assembly (left) or in a parallel pathway (right) to inhibit Rac*. (B) WT (black curve) and *ARHGAP15-null* cells (dark blue dashed curve) were first treated with an actin polymerization inhibitor (10 μM latrunculin B [Lat-B]) and then were treated with red light for 10 min. Rac* was measured as in Fig. 4 C. Each point represents a mean of three independent experiments. (C) *ARHGAP15-null* cells in the absence (light blue dashed curve) or presence of 10 μM latrunculin B (dark blue dashed curve) were treated with red light for 10 min. Rac* was measured as in Fig. 4 C. Each point represents a mean of three independent experiments. Our observation that disruption of ArhGAP15 and actin polymerization yielded compounded defects when combined suggests that they act in parallel pathways (Fig. 8 A, right). Error bars indicate SEM. *, P < 0.05 by unpaired *t* test. Immunoblots depict one representative experiment. Molecular masses are given in kilodaltons.

ARHGAP15-null cells (Fig. S5). We also performed analogous experiments in our *SH3BP1-null* line; however, Rac* activity in these cells was minimally perturbed compared with *ARH GAP15-null* cells, though there was a small but statistically significant elevation of Rac* activity at the 0.5-min time point, suggesting a lesser role for this GAP (Fig. S6, B and C).

As our earlier experiments indicated that actin assembly is also a negative regulator of PIP$_3$-driven Rac* activity (Fig. 6), we next tested whether actin assembly and ArhGAP15 function through the same or independent pathways to turn off Rac*. If actin assembly and ArhGAP15 function in the same pathway, disruption of both should produce similar defects in Rac* activity when compared with disrupting either alone (Fig. 8 A, left). In contrast, if actin assembly and ArhGAP15 primarily function in nonoverlapping pathways, disruption of both should lead to compounded defects in Rac* regulation (Fig. 8 A, right). We found that latrunculin-treated *ARHGAP15-null* cells produced significantly higher levels of phospho-Pak than latrunculin-treated WT cells (Fig. 8 B). Similarly, latrunculin-treated *ARHGAP15-null* cells showed more severe defects in Rac* turnoff than nontreated *ARHGAP15-null* cells (Fig. 8 C). Collectively, these results indi-

cate that actin assembly and ArhGAP15 function in parallel pathways to inhibit Rac* activity.
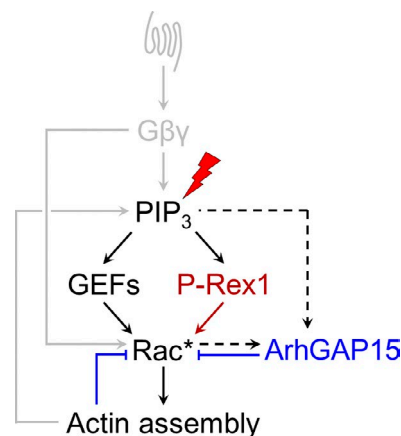
Discussion

The signaling cascades for eukaryotic chemotaxis contain numerous positive and negative feedback loops, parallel pathways, and components that are reused in multiple circuits. As a result, it has been difficult to uncover the logic of individual modules within the signaling network. In this study, we used a combination of optogenetics, pharmacology, and CRISPR-based knockout to isolate and interrogate individual nodes in the cascade, with a focus on identifying the signaling steps that mediate neutrophil adaptation. We focused on the phospholipid PIP$_3$ and the small GTPase Rac as each plays a prominent role in driving neutrophil chemotaxis. PIP$_3$ is a particularly prominent regulator of the migration program; this lipid is critical for neutrophil migration in vivo (Yoo et al., 2010) and for polarization of neutrophils in suspension (Ferguson et al., 2007). Furthermore, uniform increases in PIP$_3$ stimulate cell polarization

in neutrophils (Fig. 2; Weiner et al., 2002; Inoue and Meyer, 2008), and localized PIP$_3$ production is sufficient to guide and even repolarize neutrophil movement (Fig. 3).

PIP$_3$ is one of the first steps where sustained chemoattractant inputs are converted to transient signaling outputs, but whether this adaptation originates at the level of PIP$_3$ or other nodes is unknown. PIP$_3$ is typically depicted as an upstream activator of Rac, but feedback interactions make it difficult to pinpoint which molecules act upstream or downstream in the actual signaling cascade (Weiner et al., 2002; Inoue and Meyer, 2008; Nguyen et al., 2016). By using our opto-PI3K input (Fig. 1), we initiated sustained PIP$_3$ generation (bypassing the normally complex regulation of PI3K) and assayed the dynamics of Rac* activation. We found that delivery of a sustained step increase in PIP$_3$ levels resulted in only transient Rac* activation (Fig. 4). This is a nonintuitive result: prior experiments using chemoattractant have shown that PIP$_3$ and Rac* levels closely follow one another in time (Benard et al., 1999; Cadwallader et al., 2002; Weiner et al., 2006) and have led to models wherein PIP$_3$ and Rac* operate within an interdependent feedback loop. Using our opto-PI3K tool to deliver a step input of PIP$_3$ to cells, we revisited these models and found that instantaneous PIP$_3$ levels do not dictate instantaneous Rac* levels. The history of activation matters, and sustained PIP$_3$ produces only transient activation of Rac. Although we focused on temporal signal processing in this study, in future work, it will be interesting to investigate how spatial changes in PIP$_3$ are converted to spatial changes in Rac*.

Proper adaptation of Rac* to PIP$_3$ requires Rac activation primarily by the GEF P-Rex1 (Figs. 5 and 9) and Rac inhibition through both the GAP ArhGAP15 and actin polymerization (Figs. 6, 7, 8, and 9). ArhGAP15 and actin polymerization function via independent pathways (Fig. 9, blue connectors) to ensure proper Rac* turnoff in response to persistent PIP$_3$ production. Whether ArhGAP15 is activated directly by PIP$_3$ or responds to downstream signals is an open question. As ArhGAP15 directly binds PIP$_3$ using its pleckstrin homology domain (Seoh et al., 2003), its GAP activity may be triggered by PIP$_3$ production (i.e., it may function in an incoherent feedforward loop to turn off Rac*). Alternatively (or additionally), as both Rac* and ArhGAP15 bind the same domain of the Rac effector Pak (Radu et al., 2013), full ArhGAP15 activity may rely on Pak-mediated negative feedback (Fig. 9, black dashed connectors), in which case ArhGAP15 stimulation could be triggered by Rac activation.

How might actin assembly negatively regulate Rac activity? One attractive class of models involves actin-dependent GAP recruitment to the plasma membrane, as similar mechanisms have been reported in other systems (Soderling et al., 2002; Mason et al., 2011). Additionally, as Rac* activity is blocked by actin assembly–dependent increases in membrane tension (Houk et al., 2012), loss of actin polymerization would disrupt or potentiate any Rac* regulators whose activities are membrane tension–dependent. One possible candidate that could act in such a manner is phospholipase D2, a Rac2 GEF (Mahankali et al., 2011) that functions in a membrane tension–sensing pathway to drive neutrophil polarization (Diz-Muñoz et al., 2016). It is important to note that although the Rac* regulators we identified in this study are PIP$_3$ driven, these factors may not necessarily be exclusive to the PIP$_3$ pathway, particularly for the effectors that may be responding to Rac activation or actin polymerization, which are shared by many chemoattractant pathways (Bengtsson et al., 1990; Downey et al., 1992; Ferguson et al., 2007).

Our observations that actin assembly serves as a potent negative regulator of PIP$_3$-driven Rac* activity run counter to previous studies wherein PIP$_3$, Rac*, and actin assembly have been generally proposed to operate within a mutual positive feedback loop (Wang et al., 2002; Weiner et al., 2002; Inoue and Meyer, 2008; Yang et al., 2012; Nguyen et al., 2016). One possible explanation for this discrepancy would be the existence of both positive and negative feedback from actin onto different upstream nodes of the chemotactic signaling cascade. For cells stimulated at the level of the receptor, latrunculin treatment would be expected to block all actin assembly–dependent regulatory pathways, including those that positively regulate Rac* activity (like actin polymerization–stimulated PIP$_3$ production). In this case, the lack of a defect in Rac* for chemoattractant-stimulated cells could be caused by ablating the roles of actin assembly in both positive (PIP$_3$) and negative (Rac based) feedback that may cancel each other out. However, when PIP$_3$ levels were held high using opto-PI3K, we eliminated the role of actin assembly in stimulating PIP$_3$ production, facilitating the isolation of actin assembly's inhibitory effects on Rac* activity. Importantly, although we identify a global negative role for actin polymerization with regard to Rac activation, this is not incompatible with previous studies showing a local positive role of actin polymer for leading edge signals (Wang et al., 2014; Nguyen et al., 2016); indeed, this local positive global negative logic is central to many models of cell polarity.

Like many other signaling pathways, the chemotactic cascade exhibits significant redundancy in which knockout of individual effectors often results in no more than minor defects. However, simultaneous disruption of multiple such effectors produces far more profound phenotypes (Witke et al., 1992; Falk et al., 2003; Chen et al., 2007; van Haastert

Figure 9. **Model for PIP$_3$-driven Rac regulation.** The Rac GEF P-Rex1 (red connector) is the major (though not only) PIP$_3$-activated Rac GEF. Downstream of Rac*, actin polymerization and ArhGAP15 function in parallel pathways (blue connectors) to inhibit Rac*. ArhGAP15 activity may require Rac* or be stimulated independently (black dashed arrows). Our data and previous studies are consistent with ArhGAP15 functioning in a negative feedback loop and/or an incoherent feedforward loop to regulate Rac (Costa et al., 2007; Radu et al., 2013). These interactions are masked by additional feedback and redundancy (gray arrows) when input is delivered at the level of the chemoattractant receptor but are revealed when input is delivered at the level of PIP$_3$ production via optogenetics (red lightning bolt).

et al., 2007; Rericha and Parent, 2008; Van Haastert, 2010). Dissecting these pathways has typically relied on knocking out obvious homologues in tandem or performing enhancer/suppresser screens in the background of individual mutants. In this study, we used a complementary approach using optogenetics to activate downstream nodes of the chemotactic signaling network. The PIP_3-driven components we identified through this strategy remain relevant in the context of the overall cascade despite their roles in Rac regulation being masked when input was provided at the receptor. Although knockout of P-Rex1 yielded a minimal phenotype on its own for chemoattractant-stimulated cells, it produced a significant phenotype when knocked out in tandem with Vav1; notably, Vav1 also gave minimal phenotypes on its own, supporting the idea of redundant activation of Rac through these two effectors (Lawson et al., 2011). Although we did not observe significant defects in chemoattractant-driven Rac activation for *ARHGAP15-null* cells in vitro, ArhGAP15 plays an important role in regulating neutrophil migration from bone marrow in mice in vivo (Campa et al., 2016).

Although we have defined major players mediating Rac* adaptation in response to PIP_3, our findings do not preclude the possibility of additional adaptive circuits operating at distinct or overlapping portions of the network. For example, the bacterial chemotactic signaling cascade contains multiple independently adapting subcircuits. At the top of the cascade, the bacterial chemosensory receptors use posttranslational negative feedback to measure whether the cells are moving up or down agonist gradients (Barkai and Leibler, 1997). More recent work has uncovered an additional adaptive circuit operating further downstream at the level of the flagellar motor proteins. This second adaptive circuit operates on a time scale of minutes (rather than seconds for the receptors) and is essential for ensuring that the signaling outputs are well tuned to the dynamic range of the inputs (Yuan et al., 2012; Yuan and Berg, 2013). Similarly, the PIP_3–Rac circuit we identify in this study is likely not acting alone and may collaborate with other adaptive steps at the level of the receptor (Brzostowski et al., 2013) and other portions of the cascade (Iijima and Devreotes, 2002; Weiner et al., 2007; Zhang et al., 2008).

Our approach of using optogenetics to isolate and dissect a signaling module enabled us to uncover a temporal integration circuit whose logic was masked when inputs were provided at the level of the receptor. This strategy should prove powerful for deconvolving other signaling networks that contain redundant pathways and complex feedback interactions.

Materials and methods

Cell culture
HL-60 cells were grown in RPMI 1640 media supplemented with L-glutamine and 25 mM Hepes (Mediatech) and containing 10% (vol/vol) heat-inactivated fetal bovine serum (Gibco). Cultures were maintained at a density of 0.2–1.0 million cells/ml at 37°C/5% CO_2. dHL-60s were obtained by adding 1.5% (vol/vol) DMSO (Sigma-Aldrich) to actively growing cells followed by incubation for an additional 5 d. Note that unless otherwise stated, all experiments used dHL-60s expressing our optogenetic system for controlling PI3K activity. HEK293T cells (used to generate lentivirus for transduction of HL-60 cells) were grown in DMEM (Mediatech) containing 10% (vol/vol) heat-inactivated fetal bovine serum and maintained at 37°C/5% CO_2.

Plasmids
Vectors for mammalian expression of PhyB-mCherry-CAAX (used in the experiments described in Figs. 1 and 2) and iSH2-YFP-PIF have been described previously (Toettcher et al., 2011). To generate a vector expressing short-PhyB–mCherry-CAAX (used in experiments described in Figs. 3 and 4), PhyB-mCherry-CAAX was released from its pHR backbone via digestion with MluI and NotI. Short-PhyB (residues 1–621 of PhyB), mCherry, and the CAAX motif from KRas were then PCR amplified and ligated into the pHR backbone via Gibson assembly (Gibson et al., 2009). A gRNA with homology to exon 2 of *PREX1* (5′-GCATCGCATCCG GCAGAACG-3′) was cloned into the previously described LentiGuide-Puro backbone (52963; Addgene; Sanjana et al., 2014). gRNAs used to generate our *PREX1-null–2* (5′-GCAACCATGAGA AAGCCCTG-3′), *ARHGAP15-null* (5′-AATTCTACCCGCCAA GGCAC-3′), and *SH3BP1-null* (5′-CAGGAACTCAGCGGTCTC CG-3′) cell lines were also cloned into LentiGuide-Puro. A vector expressing human codon–optimized *Streptococcus pyogenes* Cas9 with a C-terminal tagBFP fusion was a gift from S. Qi (Stanford University, Stanford, CA).

Transduction of HL-60 cells
HEK293T cells were seeded into six-well plates and grown until ∼80% confluent. For each well, 1.5 µg pHR vector (containing the appropriate transgene), 0.167 µg vesicular stomatitis virus–G vector, and 1.2 µg cytomegalovirus 8.91 vector were mixed and prepared for transfection using TransIT-293 transfection reagent (Mirus Bio) per the manufacturer's instructions. After transfection, cells were grown for an additional 3 d, after which virus-containing supernatants were harvested and concentrated ∼40-fold using a Lenti-X Concentrator (Takara Bio Inc.) per the manufacturer's instructions. Concentrated viruses were frozen and stored at −80°C until needed. For all transductions, thawed virus was mixed with ∼0.3 million cells in growth media supplemented with polybrene (8 µg/ml) and incubated overnight. Cells expressing desired transgenes were isolated by culturing in growth media supplemented with puromycin (1 µg/ml) or using FACS as appropriate.

Purification of PCB
25 mg of PCB (Santa Cruz Biotechnology, Inc.) was resuspended in ∼10 ml dry DMSO and purified by HPLC using an Atlantis Prep T3 OBD 5 µm, 19 × 100 mm column (Waters) equilibrated with solvent A (0.5% formic acid in water). The PCB solution was loaded onto the column at a flow rate of 15 ml/min and eluted with a gradient of 5% solvent B (0.5% formic acid in acetonitrile) for 5 min followed by 100% solvent B for 11 min. Samples were collected by hand, and those from the major peak were pooled together, lyophilized, and resuspended in dry DMSO. The concentration of PCB was determined by measuring the absorbance at 680 nm. The PCB was then diluted to 12.5 mM using dry DMSO and stored at −80°C in small aliquots.

Quantification of PhyB expression after differentiation
The percentage of undifferentiated HL-60 cells and dHL-60 cells 5 d after differentiation expressing PhyB-mCherry-CAAX was determined by flow cytometry using a FACSAria III (BD) to gate cells based on mCherry fluorescence. The fraction of dHL-60 cells retaining PhyB expression after differentiation was determined by the ratio of the percent mCherry-positive dHL-60s to the percent mCherry-positive undifferentiated HL-60s. An identical procedure was performed to measure the fraction of dHL-60 cells that retained short-PhyB–mCherry-CAAX expression after differentiation. For each condition, a minimum of 50,000 cells was analyzed.

F-actin staining

dHL-60s 5 d after differentiation were concentrated to 1.5 million cells/ml and incubated in starvation media supplemented with 4 µM PCB for 45–60 min at 37°C/5% CO_2. Cells were then illuminated with a 750-nm LED for 5 min followed by either (a) no additional treatment, (b) treatment with 10 nM fMLP for 4 min, or (c) illumination with a 650-nm LED for 6 min. Afterward, 0.5 ml of cells were fixed by the addition of 0.5 ml fixation buffer (280 mM KCl, 2 mM $MgCl_2$, 4 mM EGTA, 40 mM Hepes, 0.4% BSA, 640 mM sucrose, and 7.4% formaldehyde [wt/vol], pH 7.5) and incubated at room temperature for 15–20 min. Cells were then pelleted, washed once with intracellular buffer (140 mM KCl, 1 mM $MgCl_2$, 2 mM EGTA, 20 mM Hepes, and 0.2% BSA, pH 7.5), and resuspended in staining buffer (intracellular buffer + 66 nM rhodamine-phalloidin [Thermo Fisher Scientific] and 0.2% Triton X-100). After incubation at room temperature for 30 min, cells were pelleted and then resuspended in intracellular buffer. Cells were imaged by confocal microscopy on an Eclipse T*i* inverted microscope (Nikon) equipped with a CSU-X1 spinning disk (Yokogawa Electric Corporation), an MLC400B monolithic laser combiner with 405-, 488-, 561-, and 640-nm laser lines (Agilent Technologies), a 60× 1.4 NA Plan Apochromat objective (Nikon), and an iXon3 electron-multiplying charge-coupled device camera (Andor Technology). All microscope hardware was controlled using Nikon Elements. A user who was blinded to the experimental conditions scored the percentage of cells exhibiting polarized accumulation of filamentous actin.

Preparation of dHL-60s for live-cell imaging

Glass slides and #1.5 coverslips (22 × 22 mm) were prepared by cleaning with methanol, drying, and coating with a solution of RPMI 1640 containing 2% (wt/vol) BSA for >30 min followed by several washes with deionized water. dHL-60s 5 d after differentiation were serum starved in RPMI 1640 containing 4 µM PCB for >45 min at 37°C/5% CO_2 at a density of ~1.0 million cells/ml. For control experiments, cells were similarly prepared, but PCB was omitted from all media. Approximately 400 µl of cells was pelleted and resuspended in ~10 µl RPMI 1640 containing 0.2% (wt/vol) BSA and 10 mM EDTA. Approximately 3.5 µl of this suspension was sealed between a glass slide and coverslip using valap (a mixture of equal parts Vaseline, paraffin wax, and lanolin). We refer to this preparation as a "squeeze chamber."

Hardware setup for live-cell imaging

For experiments depicted in Fig. 2 (B and C), cells were imaged by confocal microscopy using the imaging hardware setup described in the F-actin staining section. YPF-tagged opto-PI3K was imaged every 10 s using a 488-nm laser. Activation of opto-PI3K was achieved by illuminating cells in the entire field of view for 0.5 s using a 640-nm laser at each 10-s interval. Deactivation of opto-PI3K was accomplished by placing a 725-nm longpass filter (FSQ-RG9; Newport) in the transmitted light path (gently resting on top of the condenser) and illuminating cells with the halogen lamp. The lamp was used to continuously illuminate the cells at all times, except when actively imaging opto-PI3K. All imaging was performed at room temperature.

Hardware used for the experiments depicted in Figs. 3 and S1 included an Eclipse T*i* inverted microscope equipped with a motorized laser TIRF illumination unit, a Borealis beam-conditioning unit (Andor Technology), a CSU-W1 Yokogawa spinning disk (Andor Technology), a 60× Plan Apochromat TIRF 1.49 NA objective (Nikon), an iXon Ultra electron-multiplying charge-coupled device camera, and a laser merge module (LMM5; Spectral Applied Research) equipped with 405-, 440-, 488-, 514-, and 561-nm laser lines. All hardware was controlled using Micro-Manager (University of California, San Francisco), and all experiments were performed at room temperature.

Activity of opto-PI3K was controlled via 630- (red) and 740-nm (IR) LEDs (Lightspeed Technologies), which transmitted light through a custom DMD (Andor Technology) at varying intensities by connecting the LEDs to the analogue outputs of a digital-to-analogue converter and setting the LED voltages using custom MATLAB code (MathWorks). A second IR LED of fixed intensity was attached to the DMD so that micromirrors not projecting red/IR light of varying intensities would instead continuously project light from this fixed-intensity source. Our microscope is equipped with two stacked dichroic turrets such that samples can be simultaneously illuminated with red/IR LEDs using a 620-nm shortpass dichroic filter (Chroma Technology Corp.) in the upper turret while also placing the appropriate dichroic (Chroma Technology Corp.) in the lower turret (for TIRF microscopy) or leaving it empty (for confocal microscopy).

Spatial control of opto-PI3K activity in live cells

dHL-60s and imaging hardware were prepared as described in the two preceding sections. For the experiments depicted in Figs. 3 and S1 (B and C), the DMD was configured so that a 100 × 100 array of micromirrors (illuminating a ~225 µm² area of the field of view located in roughly the center of the 800 × 600 array of the DMD) projected red/IR light from our computer-controlled LEDs, whereas the remaining micromirrors projected IR light from our fixed-intensity IR LED. Using our 514-nm laser, images of YFP-tagged opto-PI3K were acquired every 10 s for 10 min via confocal microscopy. At all times, cells were continuously illuminated with red/IR light from the DMD (see previous section for details). For the first 5 min of our 10-min time courses, our computer-controlled red and IR LEDs were set to 100% and 0% power, respectively, such that only red light was projected through the 100 × 100 array. This box was positioned over the rear third of an actively migrating dHL-60. During the second 5 min of the 10-min time courses, we swapped the orientation of opto-PI3K activity: our computer-controlled red and IR LEDs were set to 0% and 100% power, respectively, so that only IR light was projected through the 100 × 100 array and into the 225-µm² box. The fixed-intensity IR LED was manually switched off so that the remainder of the field of view was "dark." It is important to note here that green light can activate opto-PI3K, though not as potently as red light (Toettcher et al., 2011). Consequently, although we were imaging cells with our 514-nm laser, we were also simultaneously stimulating opto-PI3K activity in cells across the entire field of view (we note that opto-PI3K translocation to the membrane was observable under these conditions) except for the portion lying within the 225-µm² box of IR light. For a cell partially overlapping this box, opto-PI3K would be confined to the portion of the cell lying outside the box. For control cells where PCB was not added to the media, cells were observed for only the first 5-min period where red light was directed into the 225-µm² box and IR light was directed everywhere else.

For the experiments depicted in Fig. S1 A, the computer-controlled LEDs were placed beyond the DMD, but before the 620-nm shortpass filter, so that the entire field of view could be illuminated with red/IR light while simultaneously imaging using other wavelengths. Opto-PI3K and plasma membrane–bound PhyB-CAAX were imaged by TIRF microscopy using 514- and 561-nm lasers, respectively, every 10 s for a total of 15 min. The entire field of view was initially illuminated using only the IR LED. At 5 min, the IR LED was shut off while simultaneously switching on the red LED to stimulate opto-PI3K activity.

Image analysis

ImageJ (National Institutes of Health), CellProfiler (Broad Institute), and Excel (Microsoft) were used for all image analysis. For the experiments depicted in Fig. S1, the percent change in opto-PI3K activity was

determined by first using the TIRF footprint of the PhyB-CAAX channel to create a binary mask for the entire field of view. Within this mask, the ratio of the median opto-PI3K signal to the median PhyB-CAAX signal was plotted over time after background correction of each channel. All data are normalized relative to the 290-s time point, which was assigned a percent change of 0.

For the experiments depicted in Fig. S1 B, a 225-μm² box of red light was positioned over the rear third of an actively migrating dHL-60 cell as described in the preceding section. Cells were observed every 10 s over a 5-min window and scored as "escaping" if, by the end of this observation window, the cell body and 225-μm² box showed no overlap. The experiments depicted in Figs. 3 and S1 C were initially set up identical to those described in Fig. S1 B. However, only cells that remained within the 225-μm² box of red light for the first 5 min were scored. For each 10-s interval of the 10-min time course, the ratio of the area of the cell inside the 225-μm² box to the area of the entire cell body was calculated.

Quantification of PIP₃ by MS

dHL-60s 5 d after differentiation were serum starved by incubation in starvation media (growth media lacking fetal bovine serum) for 45–60 min at 37°C/5% CO_2 at a density of 2.0 million cells/ml. For light-based experiments, starvation media was additionally supplemented with 4 μM PCB. All time courses were performed at room temperature. For each time point, samples containing 0.6 million cells were added to ice-cold 1 M HCl, pelleted, and snap frozen in liquid N_2. MS was used to measure inositol lipid levels essentially as previously described (Clark et al., 2011) using a QTRAP 4000 (AB Sciex) mass spectrometer and using the lipid extraction and derivatization method described for cultured cells, with the modification that 10 ng C17:0/C16:0 PtdIns(3,4,5)P_3 internal standard and 10 ng C17:0/C16:0 PtdIns internal standard were added to primary extracts and that final samples were dried in a speedvac concentrator rather than under N_2. Measurements were conducted in triplicate on 0.6 million cells per sample. PIP₃ response ratios were calculated by dividing the PIP₃ response area by the PIP₃ internal standard in each sample. To account for cell input variability, these PIP₃ response ratios were then divided by the phosphatidylinositol response ratios (phosphatidylinositol response area divided by the phosphatidylinositol internal standard response area) determined for each sample.

Phospho-Akt and phospho-Pak time courses

dHL-60s (5 d after differentiation) were serum starved by incubation in starvation media (growth media lacking fetal bovine serum) for 45–60 min at 37°C/5% CO_2 at a density of 1.5 million cells/ml. All time courses were performed at room temperature. For light-based experiments, starvation media was additionally supplemented with 4 μM PCB.

For chemoattractant-based time courses (e.g., Fig. 4 E), 10 nM fMLP was then added to cells, and samples were collected at indicated time points by mixing 0.5 ml of cells with 0.5 ml ice-cold stop solution (20% TCA, 40 mM NaF, and 20 mM β-glycerophosphate). Samples were incubated at 4°C for 1–12 h, after which proteins were pelleted, washed once with 0.75 ml ice-cold 0.5% TCA, and solubilized in 2× Laemmli sample buffer (Bio-Rad Laboratories).

Light-based time courses were performed as described in the preceding paragraph with the following exception. After serum starvation, cells were illuminated with a 740-nm LED for 5 min followed by illumination with a 650-nm LED (Lightspeed Technologies) for 10 min.

Rac* pulldown assays

Rac* was isolated from whole-cell extracts using PAK-GST–coated beads essentially as previously described (Benard et al., 1999). dHL-60s (5 d after differentiation) were serum starved by incubation in starvation media (growth media lacking fetal bovine serum) for 45–60 min at 37°C/5% CO_2 at a density of 2.0 million cells/ml. For light-based experiments, starvation media was additionally supplemented with 4 μM PCB. After starvation, cells were pelleted by centrifugation at 180 g for 5 min and resuspended in mHBSS (150 mM NaCl, 4 mM KCl, 1 mM $MgCl_2$, 10 mM glucose, and 20 mM Hepes, pH 7.2) at a density of 20.0 million cells/ml. For chemoattractant-based time courses, 1,000 nM fMLP was added to the cells, samples (10 million cells each) were collected at indicated time points, and then samples were lysed with ice-cold 2× lysis buffer (1× lysis buffer: 25 mM Tris-HCl, 150 mM NaCl, 5 mM $MgCl_2$, 1% NP-40, 1 mM DTT, 5% glycerol, 1 mM PMSF, and cOmplete protease inhibitor cocktail [Roche]). Cell lysates were then centrifuged at 20,000 g for 1 min at 4°C, and supernatants were recovered, snap-frozen in liquid N_2, and stored at −80°C. Light-based time courses were performed identically, with the exception that cells were pretreated with inactivating IR light for 5 min followed by stimulation with red light.

To perform the pulldown assays, samples were thawed in a room temperature water bath and placed on ice. For each sample, 600 μg of protein was added to 10 μg PAK-GST protein beads (Cytoskeleton, Inc.). Ice-cold 1× lysis buffer was then added to each sample to bring the total reaction volume to 0.9 ml. Samples were incubated at 4°C while rotating for 1 h, followed by centrifugation at 5,000 g for 1 min at 4°C to pellet the PAK-GST beads. The supernatant was discarded, beads were washed once with wash buffer (25 mM Tris-HCl, 30 mM $MgCl_2$, and 40 mM NaCl, pH 7.5), pelleted, and then resuspended in 2× Laemmli buffer (Bio-Rad Laboratories).

Samples were subjected to SDS-PAGE followed by transfer onto PVDF membranes. Membranes were blocked for ~1 h in a 1:1 solution of TBS (20 mM Tris and 500 mM NaCl, pH 7.4) and Odyssey blocking buffer (LI-COR Biosciences) followed by overnight incubation at 4°C with Rac1/2/3 antibody (2456; Cell Signaling Technology) diluted 1:500 in a solution of 1:1 TBST (TBS + 0.2% wt/vol Tween-20) and Odyssey blocking buffer. Membranes were then washed 3× with TBST and incubated for ~1 h at room temperature with an HRP-conjugated goat anti–rabbit antibody (Thermo Fisher Scientific) diluted 1:10,000 in Odyssey blocking buffer. Membranes were then washed 3× with TBST and 1× with TBS followed by incubation with HRP substrate (SuperSignal West Dura; Thermo Fisher Scientific) for 5 min. Membranes were then dried and imaged via chemiluminescence on an Odyssey Fc (LI-COR Biosciences). Analysis was performed using Image Studio (LI-COR Biosciences).

Immunoblot assays

Protein samples in 2× Laemmli sample buffer (prepared from 0.5–1.0 million cells) were subjected to SDS-PAGE followed by transfer onto nitrocellulose membranes. Membranes were blocked for ~1 h in a 1:1 solution of TBS (20 mM Tris and 500 mM NaCl, pH 7.4) and Odyssey blocking buffer followed by overnight incubation at 4°C with primary antibodies diluted 1:1,000 in a solution of 1:1 TBST (TBS + 0.2% wt/vol Tween-20) and Odyssey blocking buffer. Membranes were then washed 3× with TBST and incubated for ~1 h at room temperature with secondary antibodies diluted 1:20,000 in Odyssey blocking buffer. Membranes were then washed 3× with TBST and 1× with TBS and then were imaged using an Odyssey Fc. Analysis was performed using Image Studio. For phospho-Pak and phospho-Akt immunoblots, the ratio of phospho-Pak to total Pak or phospho-Akt to total Akt was calculated. These values were then normalized by scaling each relative to the value of WT or non–latrunculin-treated cells at time point "1 min" for cells stimulated using opto-PI3K or "0.5 min" for cells stimulated with chemoattractant.

Primary antibodies used were phospho-Akt (Ser473; D9E) XP (4060; Cell Signaling Technology), phospho-PAK1 (Ser199/204)/PAK2 (Ser192/197; 2605; Cell Signaling Technology), Akt (pan; 40D4; 2920; Cell Signaling Technology), PAK2 (3B5; 4825; Cell Signaling Technology), PREX1 (D8O8D; 13168; Cell Signaling Technology), ARHGAP15 (N1N3; GeneTex), SH3BP1 (GeneTex), GAPDH loading control antibody (GA1R; Thermo Fisher Scientific), and monoclonal anti–β-tubulin D66 (Sigma-Aldrich). Secondary antibodies used were IRDye 680 RD goat anti–rabbit and IRDye 800 CW goat anti–mouse (LI-COR Biosciences).

Generation of knockout cell lines using CRISPR/Cas9

WT HL-60 cells were transduced with vectors containing puromycin-selectable gRNAs targeting *PREX1*, *ARHGAP15*, or *SH3BP1*. After selection, cells were then transduced with an *S. pyrogenes* Cas9 sequence fused to tagBFP. Cells expressing high levels of Cas9-tagBFP were collected using FACS, after which a heterogeneous population was obtained as assessed by immunoblot (representative example shown in Fig. S2 A) and sequencing of the genomic DNA flanking the Cas9 cut site (representative example shown in Fig. S2 B). These cells were then diluted into 96-well plates at a density of one cell/well to generate clonal lines, which were again verified by genomic DNA sequencing (representative example shown in Fig. S2 C) and immunoblot (Figs. 5 B, 7 B, S3 A, and S6 A). Note that P-Rex1 protein was no longer detectable on the immunoblot in our clonal knockout line (compare Figs. 5 B and S2 A).

To verify that a particular clonal line arose from a single cell, we isolated genomic DNA and sequenced the portion flanking the gRNA annealing site. A variable number of bases were inserted/deleted after repair of Cas9-induced double-strand breaks, and sequencing chromatograms of regions flanking the Cas9 cut site contained multiple (mixed) peaks that corresponded with the slight differences in how the double-strand break at each gRNA-targeted locus was repaired (example shown in Fig. S2 B). As HL-60 cells are pseudodiploid (Gallagher et al., 1979), each position on the chromatogram within the "mixed peaks" region should contain at most two distinct peaks, indicating a pair of edited loci (example shown in Fig. S2 C). Putative clones containing more than two peaks for a given position on their respective chromatograms could then be discarded, as they would have arisen from two or more cells seeding the same well of a 96-well plate.

Online supplemental material

Fig. S1 shows how stimulation of dHL-60s using opto-PI3K drives polarization. Fig. S2 shows validation of CRISPR-mediated genome editing in HL-60 cells. Fig. S3 shows PIP$_3$-dependent Pak phosphorylation in an independently generated *PREX1-null* cell line. Fig. S4 shows how actin depolymerization potentiates Rac activity in *PREX1-null* cells. Fig. S5 shows how *ARHGAP15-null* cells exhibit normal opto-PI3K–generated Akt phosphorylation. Fig. S6 shows how the GAP SH3BP1 plays a minor role in PIP$_3$-driven Rac activation. Videos 1 and 2 show how recruitment of opto-PI3K to the plasma membrane (global red light illumination) and off of the plasma membrane (global IR light illumination) reversibly regulates cell polarity and pseudopod formation in neutrophil-like dHL-60 cells. Videos 3 and 4 show how subcellular spatial patterning of opto-PI3K activity regulates directional movement in neutrophil-like dHL-60 cells.

Acknowledgments

References

Alessi, D.R., M. Andjelkovic, B. Caudwell, P. Cron, N. Morrice, P. Cohen, and B.A. Hemmings. 1996. Mechanism of activation of protein kinase B by insulin and IGF-1. *EMBO J.* 15:6541–6551.

Arai, H., F.S. Monteclaro, C.L. Tsou, C. Franci, and I.F. Charo. 1997. Dissociation of chemotaxis from agonist-induced receptor internalization in a lymphocyte cell line transfected with CCR2B. Evidence that directed migration does not require rapid modulation of signaling at the receptor level. *J. Biol. Chem.* 272:25037–25042. http://dx.doi.org/10.1074/jbc.272.40.25037

Artemenko, Y., T.J. Lampert, and P.N. Devreotes. 2014. Moving towards a paradigm: common mechanisms of chemotactic signaling in *Dictyostelium* and mammalian leukocytes. *Cell. Mol. Life Sci.* 71:3711–3747. http://dx.doi.org/10.1007/s00018-014-1638-8

Barkai, N., and S. Leibler. 1997. Robustness in simple biochemical networks. *Nature.* 387:913–917. http://dx.doi.org/10.1038/43199

Benard, V., B.P. Bohl, and G.M. Bokoch. 1999. Characterization of Rac and Cdc42 activation in chemoattractant-stimulated human neutrophils using a novel assay for active GTPases. *J. Biol. Chem.* 274:13198–13204. http://dx.doi.org/10.1074/jbc.274.19.13198

Bengtsson, T., E. Särndahl, O. Stendahl, and T. Andersson. 1990. Involvement of GTP-binding proteins in actin polymerization in human neutrophils. *Proc. Natl. Acad. Sci. USA.* 87:2921–2925. http://dx.doi.org/10.1073/pnas.87.8.2921

Bréchard, S., A. Salsmann, and E.J. Tschirhart. 2009. OAG induces an additional PKC-, PI3K-, and Rac2-mediated signaling pathway up-regulating NOX2 activity, independently of Ca^{2+} entry. *J. Leukoc. Biol.* 85:638–647. http://dx.doi.org/10.1189/jlb.0508330

Brzostowski, J.A., S. Sawai, O. Rozov, X.-H. Liao, D. Imoto, C.A. Parent, and A.R. Kimmel. 2013. Phosphorylation of chemoattractant receptors regulates chemotaxis, actin reorganization and signal relay. *J. Cell Sci.* 126:4614–4626. http://dx.doi.org/10.1242/jcs.122952

Buckley, C.E., R.E. Moore, A. Reade, A.R. Goldberg, O.D. Weiner, and J.D.W. Clarke. 2016. Reversible optogenetic control of subcellular protein localization in a live vertebrate embryo. *Dev. Cell.* 36:117–126. http://dx.doi.org/10.1016/j.devcel.2015.12.011

Burns, M.E., and D.A. Baylor. 2001. Activation, deactivation, and adaptation in vertebrate photoreceptor cells. *Annu. Rev. Neurosci.* 24:779–805. http://dx.doi.org/10.1146/annurev.neuro.24.1.779

Bustelo, X.R. 2014. Vav family exchange factors: an integrated regulatory and functional view. *Small GTPases.* 5:e973757. http://dx.doi.org/10.4161/21541248.2014.973757

Cadwallader, K.A., A.M. Condliffe, A. McGregor, T.R. Walker, J.F. White, L.R. Stephens, and E.R. Chilvers. 2002. Regulation of phosphatidylinositol 3-kinase activity and phosphatidylinositol 3,4,5-trisphosphate accumulation by neutrophil priming agents. *J. Immunol.* 169:3336–3344.

Campa, C.C., G. Germena, E. Ciraolo, C. Copperi, A. Sapienza, I. Franco, A. Ghigo, A. Camporeale, A. Di Savino, M. Martini, et al. 2016. Rac signal adaptation controls neutrophil mobilization from the bone marrow. *Sci. Signal.* 9:ra124. http://dx.doi.org/10.1126/scisignal.aah5882

Chen, L., M. Iijima, M. Tang, M.A. Landree, Y.E. Huang, Y. Xiong, P.A. Iglesias, and P.N. Devreotes. 2007. PLA2 and PI3K/PTEN pathways act in parallel to mediate chemotaxis. *Dev. Cell.* 12:603–614. http://dx.doi.org/10.1016/j.devcel.2007.03.005

Cicchetti, P., A.J. Ridley, Y. Zheng, R.A. Cerione, and D. Baltimore. 1995. 3BP-1, an SH3 domain binding protein, has GAP activity for Rac and

inhibits growth factor-induced membrane ruffling in fibroblasts. *EMBO J.* 14:3127–3135.

Clark, J., K.E. Anderson, V. Juvin, T.S. Smith, F. Karpe, M.J.O. Wakelam, L.R. Stephens, and P.T. Hawkins. 2011. Quantification of PtdInsP₃ molecular species in cells and tissues by mass spectrometry. *Nat. Methods.* 8:267–272. http://dx.doi.org/10.1038/nmeth.1564

Condeelis, J., A. Hall, A. Bresnick, V. Warren, R. Hock, H. Bennett, and S. Ogihara. 1988. Actin polymerization and pseudopod extension during amoeboid chemotaxis. *Cell Motil. Cytoskeleton.* 10:77–90. http://dx.doi.org/10.1002/cm.970100113

Costa, C., L. Barberis, C. Ambrogio, A.D. Manazza, E. Patrucco, O. Azzolino, P.O. Neilsen, E. Ciraolo, F. Altruda, G.D. Prestwich, et al. 2007. Negative feedback regulation of Rac in leukocytes from mice expressing a constitutively active phosphatidylinositol 3-kinase γ. *Proc. Natl. Acad. Sci. USA.* 104:14354–14359. http://dx.doi.org/10.1073/pnas.0703175104

Coué, M., S.L. Brenner, I. Spector, and E.D. Korn. 1987. Inhibition of actin polymerization by latrunculin A. *FEBS Lett.* 213:316–318. http://dx.doi.org/10.1016/0014-5793(87)81513-2

Deladeriere, A., L. Gambardella, D. Pan, K.E. Anderson, P.T. Hawkins, and L.R. Stephens. 2015. The regulatory subunits of PI3Kγ control distinct neutrophil responses. *Sci. Signal.* 8:ra8. http://dx.doi.org/10.1126/scisignal.2005564

Dhand, R., K. Hara, I. Hiles, B. Bax, I. Gout, G. Panayotou, M.J. Fry, K. Yonezawa, M. Kasuga, and M.D. Waterfield. 1994. PI 3-kinase: structural and functional analysis of intersubunit interactions. *EMBO J.* 13:511–521.

Diz-Muñoz, A., K. Thurley, S. Chintamen, S.J. Altschuler, L.F. Wu, D.A. Fletcher, and O.D. Weiner. 2016. Membrane tension acts through PLD2 and mTORC2 to limit actin network assembly during neutrophil migration. *PLoS Biol.* 14:e1002474. http://dx.doi.org/10.1371/journal.pbio.1002474

Donald, S., K. Hill, C. Lecureuil, R. Barnouin, S. Krugmann, W. John Coadwell, S.R. Andrews, S.A. Walker, P.T. Hawkins, L.R. Stephens, and H.C.E. Welch. 2004. P-Rex2, a new guanine-nucleotide exchange factor for Rac. *FEBS Lett.* 572:172–176. http://dx.doi.org/10.1016/j.febslet.2004.06.096

Downey, G.P., C.K. Chan, P. Lea, A. Takai, and S. Grinstein. 1992. Phorbol ester-induced actin assembly in neutrophils: role of protein kinase C. *J. Cell Biol.* 116:695–706. http://dx.doi.org/10.1083/jcb.116.3.695

Falk, D.L., D. Wessels, L. Jenkins, T. Pham, S. Kuhl, M.A. Titus, and D.R. Soll. 2003. Shared, unique and redundant functions of three members of the class I myosins (MyoA, MyoB and MyoF) in motility and chemotaxis in *Dictyostelium. J. Cell Sci.* 116:3985–3999. http://dx.doi.org/10.1242/jcs.00696

Ferguson, G.J., L. Milne, S. Kulkarni, T. Sasaki, S. Walker, S. Andrews, T. Crabbe, P. Finan, G. Jones, S. Jackson, et al. 2007. PI(3)Kγ has an important context-dependent role in neutrophil chemokinesis. *Nat. Cell Biol.* 9:86–91. http://dx.doi.org/10.1038/ncb1517

Fuhler, G.M., A.L. Drayer, S.G.M. Olthof, J.J. Schuringa, P.J. Coffer, and E. Vellenga. 2008. Reduced activation of protein kinase B, Rac, and F-actin polymerization contributes to an impairment of stromal cell-derived factor-1-induced migration of CD34+ cells from patients with myelodysplasia. *Blood.* 111:359–368. http://dx.doi.org/10.1182/blood-2006-11-060632

Gallagher, R., S. Collins, J. Trujillo, K. McCredie, M. Ahearn, S. Tsai, R. Metzgar, G. Aulakh, R. Ting, F. Ruscetti, and R. Gallo. 1979. Characterization of the continuous, differentiating myeloid cell line (HL-60) from a patient with acute promyelocytic leukemia. *Blood.* 54:713–733.

Gibson, D.G., L. Young, R.-Y. Chuang, J.C. Venter, C.A. Hutchison III, and H.O. Smith. 2009. Enzymatic assembly of DNA molecules up to several hundred kilobases. *Nat. Methods.* 6:343–345. http://dx.doi.org/10.1038/nmeth.1318

Hauert, A.B., S. Martinelli, C. Marone, and V. Niggli. 2002. Differentiated HL-60 cells are a valid model system for the analysis of human neutrophil migration and chemotaxis. *Int. J. Biochem. Cell Biol.* 34:838–854. http://dx.doi.org/10.1016/S1357-2725(02)00010-9

Houk, A.R., A. Jilkine, C.O. Mejean, R. Boltyanskiy, E.R. Dufresne, S.B. Angenent, S.J. Altschuler, L.F. Wu, and O.D. Weiner. 2012. Membrane tension maintains cell polarity by confining signals to the leading edge during neutrophil migration. *Cell.* 148:175–188. http://dx.doi.org/10.1016/j.cell.2011.10.050

Hresko, R.C., H. Murata, and M. Mueckler. 2003. Phosphoinositide-dependent kinase-2 is a distinct protein kinase enriched in a novel cytoskeletal fraction associated with adipocyte plasma membranes. *J. Biol. Chem.* 278:21615–21622. http://dx.doi.org/10.1074/jbc.M302937200

Hsu, M.H., S.C. Chiang, R.D. Ye, and E.R. Prossnitz. 1997. Phosphorylation of the *N*-formyl peptide receptor is required for receptor internalization but not chemotaxis. *J. Biol. Chem.* 272:29426–29429. http://dx.doi.org/10.1074/jbc.272.47.29426

Huang, C.-H., M. Tang, C. Shi, P.A. Iglesias, and P.N. Devreotes. 2013. An excitable signal integrator couples to an idling cytoskeletal oscillator to drive cell migration. *Nat. Cell Biol.* 15:1307–1316. http://dx.doi.org/10.1038/ncb2859

Iijima, M., and P. Devreotes. 2002. Tumor suppressor PTEN mediates sensing of chemoattractant gradients. *Cell.* 109:599–610. http://dx.doi.org/10.1016/S0092-8674(02)00745-6

Inoue, T., and T. Meyer. 2008. Synthetic activation of endogenous PI3K and Rac identifies an *AND*-gate switch for cell polarization and migration. *PLoS One.* 3:e3068. http://dx.doi.org/10.1371/journal.pone.0003068

Janetopoulos, C., T. Jin, and P. Devreotes. 2001. Receptor-mediated activation of heterotrimeric G-proteins in living cells. *Science.* 291:2408–2411. http://dx.doi.org/10.1126/science.1055835

Kae, H., C.J. Lim, G.B. Spiegelman, and G. Weeks. 2004. Chemoattractant-induced Ras activation during *Dictyostelium* aggregation. *EMBO Rep.* 5:602–606. http://dx.doi.org/10.1038/sj.embor.7400151

Kim, J.-Y., R.D.M. Soede, P. Schaap, R. Valkema, J.A. Borleis, P.J. Van Haastert, P.N. Devreotes, and D. Hereld. 1997. Phosphorylation of chemoattractant receptors is not essential for chemotaxis or termination of G-protein-mediated responses. *J. Biol. Chem.* 272:27313–27318. http://dx.doi.org/10.1074/jbc.272.43.27313

Koronakis, V., P.J. Hume, D. Humphreys, T. Liu, O. Hørning, O.N. Jensen, and E.J. McGhie. 2011. WAVE regulatory complex activation by cooperating GTPases Arf and Rac1. *Proc. Natl. Acad. Sci. USA.* 108:14449–14454. http://dx.doi.org/10.1073/pnas.1107666108

Lawson, C.D., S. Donald, K.E. Anderson, D.T. Patton, and H.C.E. Welch. 2011. P-Rex1 and Vav1 cooperate in the regulation of formyl-methionyl-leucyl-phenylalanine-dependent neutrophil responses. *J. Immunol.* 186:1467–1476. http://dx.doi.org/10.4049/jimmunol.1002738

Levskaya, A., O.D. Weiner, W.A. Lim, and C.A. Voigt. 2009. Spatiotemporal control of cell signalling using a light-switchable protein interaction. *Nature.* 461:997–1001. http://dx.doi.org/10.1038/nature08446

Mahankali, M., H.-J. Peng, K.M. Henkels, M.C. Dinauer, and J. Gomez-Cambronero. 2011. Phospholipase D2 (PLD2) is a guanine nucleotide exchange factor (GEF) for the GTPase Rac2. *Proc. Natl. Acad. Sci. USA.* 108:19617–19622. http://dx.doi.org/10.1073/pnas.1114692108

Malawista, S.E., and A. de Boisfleury Chevance. 1997. Random locomotion and chemotaxis of human blood polymorphonuclear leukocytes (PMN) in the presence of EDTA: PMN in close quarters require neither leukocyte integrins nor external divalent cations. *Proc. Natl. Acad. Sci. USA.* 94:11577–11582. http://dx.doi.org/10.1073/pnas.94.21.11577

Mason, F.M., E.G. Heimsath, H.N. Higgs, and S.H. Soderling. 2011. Bi-modal regulation of a formin by srGAP2. *J. Biol. Chem.* 286:6577–6586. http://dx.doi.org/10.1074/jbc.M110.190397

Nguyen, T.T.T., W.S. Park, B.O. Park, C.Y. Kim, Y. Oh, J.M. Kim, H. Choi, T. Kyung, C.-H. Kim, G. Lee, et al. 2016. PLEKHG3 enhances polarized cell migration by activating actin filaments at the cell front. *Proc. Natl. Acad. Sci. USA.* 113:10091–10096. http://dx.doi.org/10.1073/pnas.1604720113

Ni, M., J.M. Tepperman, and P.H. Quail. 1999. Binding of phytochrome B to its nuclear signalling partner PIF3 is reversibly induced by light. *Nature.* 400:781–784. http://dx.doi.org/10.1038/23500

Porter, S.L., G.H. Wadhams, and J.P. Armitage. 2011. Signal processing in complex chemotaxis pathways. *Nat. Rev. Microbiol.* 9:153–165. http://dx.doi.org/10.1038/nrmicro2505

Radu, M., S.J. Rawat, A. Beeser, A. Iliuk, W.A. Tao, and J. Chernoff. 2013. ArhGAP15, a Rac-specific GTPase-activating protein, plays a dual role in inhibiting small GTPase signaling. *J. Biol. Chem.* 288:21117–21125. http://dx.doi.org/10.1074/jbc.M113.459719

Rericha, E.C., and C.A. Parent. 2008. Steering in quadruplet: The complex signaling pathways directing chemotaxis. *Sci. Signal.* 1:pe26. http://dx.doi.org/10.1126/scisignal.122pe26

Sanjana, N.E., O. Shalem, and F. Zhang. 2014. Improved vectors and genome-wide libraries for CRISPR screening. *Nat. Methods.* 11:783–784. http://dx.doi.org/10.1038/nmeth.3047

Schlam, D., R.D. Bagshaw, S.A. Freeman, R.F. Collins, T. Pawson, G.D. Fairn, and S. Grinstein. 2015. Phosphoinositide 3-kinase enables phagocytosis of large particles by terminating actin assembly through Rac/Cdc42 GTPase-activating proteins. *Nat. Commun.* 6:8623. http://dx.doi.org/10.1038/ncomms9623

Seoh, M.L., C.H. Ng, J. Yong, L. Lim, and T. Leung. 2003. ArhGAP15, a novel human RacGAP protein with GTPase binding property. *FEBS Lett.* 539:131–137. http://dx.doi.org/10.1016/S0014-5793(03)00213-8

Soderling, S.H., K.L. Binns, G.A. Wayman, S.M. Davee, S.H. Ong, T. Pawson, and J.D. Scott. 2002. The WRP component of the WAVE-1 complex

attenuates Rac-mediated signalling. *Nat. Cell Biol.* 4:970–975. http://dx .doi.org/10.1038/ncb886

Srinivasan, S., F. Wang, S. Glavas, A. Ott, F. Hofmann, K. Aktories, D. Kalman, and H.R. Bourne. 2003. Rac and Cdc42 play distinct roles in regulating PI(3,4,5)P$_3$ and polarity during neutrophil chemotaxis. *J. Cell Biol.* 160:375–385. http://dx.doi.org/10.1083/jcb.200208179

Stephens, L., A. Eguinoa, S. Corey, T. Jackson, and P.T. Hawkins. 1993. Receptor stimulated accumulation of phosphatidylinositol (3,4,5)-trisphosphate by G-protein mediated pathways in human myeloid derived cells. *EMBO J.* 12:2265–2273.

Takeda, K., D. Shao, M. Adler, P.G. Charest, W.F. Loomis, H. Levine, A. Groisman, W.-J. Rappel, and R.A. Firtel. 2012. Incoherent feedforward control governs adaptation of activated Ras in a eukaryotic chemotaxis pathway. *Sci. Signal.* 5:ra2. http://dx.doi.org/10.1126/scisignal.2002413

Tang, M., M. Wang, C. Shi, P.A. Iglesias, P.N. Devreotes, and C.-H. Huang. 2014. Evolutionarily conserved coupling of adaptive and excitable networks mediates eukaryotic chemotaxis. *Nat. Commun.* 5:5175. http:// dx.doi.org/10.1038/ncomms6175

Toettcher, J.E., D. Gong, W.A. Lim, and O.D. Weiner. 2011. Light-based feedback for controlling intracellular signaling dynamics. *Nat. Methods.* 8:837–839. http://dx.doi.org/10.1038/nmeth.1700

Toettcher, J.E., O.D. Weiner, and W.A. Lim. 2013. Using optogenetics to interrogate the dynamic control of signal transmission by the Ras/Erk module. *Cell.* 155:1422–1434. http://dx.doi.org/10.1016/j.cell.2013.11 .004

Van Haastert, P.J.M. 2010. Chemotaxis: insights from the extending pseudopod. *J. Cell Sci.* 123:3031–3037. http://dx.doi.org/10.1242/jcs.071118

van Haastert, P.J.M., I. Keizer-Gunnink, and A. Kortholt. 2007. Essential role of PI3-kinase and phospholipase A2 in *Dictyostelium discoideum* chemotaxis. *J. Cell Biol.* 177:809–816. http://dx.doi.org/10.1083/jcb .200701134

Wang, F., P. Herzmark, O.D. Weiner, S. Srinivasan, G. Servant, and H.R. Bourne. 2002. Lipid products of PI(3)Ks maintain persistent cell polarity and directed motility in neutrophils. *Nat. Cell Biol.* 4:513–518. http://dx.doi .org/10.1038/ncb810

Wang, M.-J., Y. Artemenko, W.-J. Cai, P.A. Iglesias, and P.N. Devreotes. 2014. The directional response of chemotactic cells depends on a balance between cytoskeletal architecture and the external gradient. *Cell Reports.* 9:1110–1121. http://dx.doi.org/10.1016/j.celrep.2014.09.047

Watanabe, M., M. Terasawa, K. Miyano, T. Yanagihara, T. Uruno, F. Sanematsu, A. Nishikimi, J.-F. Côté, H. Sumimoto, and Y. Fukui. 2014. DOCK2 and DOCK5 act additively in neutrophils to regulate chemotaxis, superoxide production, and extracellular trap formation. *J. Immunol.* 193:5660–5667. http://dx.doi.org/10.4049/jimmunol.1400885

Weiner, O.D., P.O. Neilsen, G.D. Prestwich, M.W. Kirschner, L.C. Cantley, and H.R. Bourne. 2002. A PtdInsP$_3$- and Rho GTPase-mediated positive feedback loop regulates neutrophil polarity. *Nat. Cell Biol.* 4:509–513. http://dx.doi.org/10.1038/ncb811

Weiner, O.D., M.C. Rentel, A. Ott, G.E. Brown, M. Jedrychowski, M.B. Yaffe, S.P. Gygi, L.C. Cantley, H.R. Bourne, and M.W. Kirschner. 2006. Hem-1 complexes are essential for Rac activation, actin polymerization, and myosin regulation during neutrophil chemotaxis. *PLoS Biol.* 4:e38. http ://dx.doi.org/10.1371/journal.pbio.0040038

Weiner, O.D., W.A. Marganski, L.F. Wu, S.J. Altschuler, and M.W. Kirschner. 2007. An actin-based wave generator organizes cell motility. *PLoS Biol.* 5:e221. http://dx.doi.org/10.1371/journal.pbio.0050221

Welch, H.C.E., W.J. Coadwell, C.D. Ellson, G.J. Ferguson, S.R. Andrews, H. Erdjument-Bromage, P. Tempst, P.T. Hawkins, and L.R. Stephens. 2002. P-Rex1, a PtdIns(3,4,5)P$_3$- and Gβγ-regulated guanine-nucleotide exchange factor for Rac. *Cell.* 108:809–821. http://dx.doi.org/10.1016/ S0092-8674(02)00663-3

Witke, W., M. Schleicher, and A.A. Noegel. 1992. Redundancy in the microfilament system: Abnormal development of dictyostelium cells lacking two F-actin cross-linking proteins. *Cell.* 68:53–62. http://dx.doi .org/10.1016/0092-8674(92)90205-Q

Xu, X., M. Meier-Schellersheim, X. Jiao, L.E. Nelson, and T. Jin. 2005. Quantitative imaging of single live cells reveals spatiotemporal dynamics of multistep signaling events of chemoattractant gradient sensing in *Dictyostelium*. *Mol. Biol. Cell.* 16:676–688. http://dx.doi.org/10.1091/ mbc.E04-07-0544

Yang, H.W., M.-G. Shin, S. Lee, J.-R. Kim, W.S. Park, K.-H. Cho, T. Meyer, and W.D. Heo. 2012. Cooperative activation of PI3K by Ras and Rho family small GTPases. *Mol. Cell.* 47:281–290. http://dx.doi.org/10.1016 /j.molcel.2012.05.007

Yi, T.M., Y. Huang, M.I. Simon, and J. Doyle. 2000. Robust perfect adaptation in bacterial chemotaxis through integral feedback control. *Proc. Natl. Acad. Sci. USA.* 97:4649–4653. http://dx.doi.org/10.1073/pnas.97.9.4649

Yoo, S.K., Q. Deng, P.J. Cavnar, Y.I. Wu, K.M. Hahn, and A. Huttenlocher. 2010. Differential regulation of protrusion and polarity by PI3K during neutrophil motility in live zebrafish. *Dev. Cell.* 18:226–236. http://dx.doi .org/10.1016/j.devcel.2009.11.015

Yuan, J., and H.C. Berg. 2013. Ultrasensitivity of an adaptive bacterial motor. *J. Mol. Biol.* 425:1760–1764. http://dx.doi.org/10.1016/j.jmb.2013.02 .016

Yuan, J., R.W. Branch, B.G. Hosu, and H.C. Berg. 2012. Adaptation at the output of the chemotaxis signalling pathway. *Nature.* 484:233–236. http://dx.doi .org/10.1038/nature10964

Zhang, S., P.G. Charest, and R.A. Firtel. 2008. Spatiotemporal regulation of Ras activity provides directional sensing. *Curr. Biol.* 18:1587–1593. http://dx .doi.org/10.1016/j.cub.2008.08.069

Zigmond, S.H. 1977. Ability of polymorphonuclear leukocytes to orient in gradients of chemotactic factors. *J. Cell Biol.* 75:606–616. http://dx.doi .org/10.1083/jcb.75.2.606

Zigmond, S.H., and S.J. Sullivan. 1979. Sensory adaptation of leukocytes to chemotactic peptides. *J. Cell Biol.* 82:517–527. http://dx.doi.org/10.1083 /jcb.82.2.517